PHOTONICS Research

Inorganic halide perovskites for lighting and visible light communication

SHUANGYI ZHAO,† QIONGHUA MO,† BAIQIAN WANG, WENSI CAI, RU LI, AND ZHIGANG ZANG*

Key Laboratory of Optoelectronic Technology & Systems (Ministry of Education), Chongqing University, Chongqing 400044, China
*Corresponding author: zangzg@cqu.edu.cn

Received 18 November 2021; revised 12 January 2022; accepted 13 January 2022; posted 14 January 2022 (Doc. ID 450483); published 25 March 2022

Inorganic halide perovskites (IHPs) have received substantial attention due to their unique optoelectronic properties. Among all the intriguing performance, the efficient luminescence of IHPs enables the practical application of white light-emitting diodes (WLEDs) for lighting. During the last decade, IHP-based white lighting sources with a high luminesce and a broad color gamut have been developed as strong competitors to conventional and classic WLEDs based on rare-earth phosphors and blue LED chips. Thus, it inspires us to give an overview of the emerging progress of IHP WLEDs that can function as lighting sources. Here, in this review, the generation of luminescent properties and white light in IHPs are first presented. Then, both photoluminescence and electroluminescence WLEDs with IHPs emitters, including both lead-based and lead-free IHPs, are synthetically discussed to exhibit their advantages. Furthermore, the efforts on the optical performance enhancement of IHPs in WLEDs are demonstrated and summarized. Apart from WLEDs, visible light communication based on IHPs featuring efficient luminescence is proposed to highlight their promising potential in lighting communication. Finally, some perspectives on the evolution and challenges are described, followed by an inspirational outlook on their future development.

https://doi.org/10.1364/PRJ.450483

1. INTRODUCTION

Since more than 20% of global electric energy is consumed by lighting every year, it is quite urgent to develop efficient lighting sources to save massive energy. White light-emitting diodes (WLEDs), which are regarded as bright and solid-state lighting sources, have aroused wide attention due to their high luminous efficiency, long operating lifetime, and ecofriendly nature [1–5]. The performance of photoluminescence and electroluminescence WLEDs, in which the white light originates from optical pump and electrical driving, is dominated by the emitters and luminescent materials [6]. In conventional WLEDs, the white emission derives from rare-earth phosphors and blue/violet InGaN/GaN LED chips. Despite the fascinating characteristics of WLEDs based on rare-earth phosphors, their further development and commercialization still suffer from the supply shortage issues of the rare-earth elements as well as the complex and high-temperature preparation processes of phosphors with energy consumption. Apart from rare-earth phosphors, organic and II-VI-/III-V group semiconductors could also be used as emitters in WLEDs; however, the instability issue of organic semiconductors and the sophisticated mass production of II-VI-/III-V semiconductors have limited their studies [7,8]. Thus, it is of great interest to explore emitting materials with feasible preparation, efficient luminescence, and excellent stability for the next-generation WLEDs applications.

Owing to the high photoluminescence quantum yield (PLQY), tunable photoluminescence (PL) across the entire visible region, and being solution-processable, inorganic halide perovskites (IHPs) have been selected over other efficient emitters in optoelectronic applications [9–11]. Moreover, compared to hybrid organic perovskites with inorganic groups, such as MA, FA, and PEA, IHPs containing stable Cs^+, Rb^+, and K^+ exhibit enhanced stability against heat, humidity, and UV irradiation. In addition, their prominent advantages, including structural stability and processability, inspire researchers to focus on their development and applications. The Goldschmit's tolerance factor (t) that depends on the ionic radius is used to estimate the structural stability of perovskites [12,13]. Thus, the organic groups with a large ionic radius indicate large t values in hybrid perovskites, resulting in the instable structures, while the Cs^+, Rb^+, and K^+ ions with a suitable radius facilitate the stabilization of the crystal structures of inorganic perovskites, leading to the improvement of structural stability. Apart from structural stability, owing to the high boiling point of inorganic ions, the high-quality IHPs can be synthesized by solution methods at increasing temperature. These properties endow IHPs with great potential for lighting, with encouraging research progresses in IHP-based lighting being witnessed in recent years. However, the practical applications of WLEDs based on inorganic lead halide perovskites ($CsPbX_3$) are still hindered by their intrinsic instability and the relatively low PLQY of red and blue emission. To obviate these problems, beneficial strategies, including coating, embedding, morphological optimization, and surface-ligand modification, are exploited to further enhance the stability and optical properties of IHPs [14–16]. In addition, it is essential for state-of-the-art WLEDs to possess broad spectra covering the entire visible region, but the narrow emission spectra of $CsPbX_3$ are identified as a major bottleneck in the lighting application. The expanded width of the emission spectra of WLEDs can be accompanied by combining with other emitters with complementary emissive spectra and incorporating dopants into IHPs to introduce novel emission peaks [17,18]. Moreover, benefiting from the fascinating characteristics of broad emission and nontoxicity, inorganic lead-free halide perovskites have emerged as good candidates for emitters in WLEDs [19–22]. Therefore, among the emitters used in high-performance WLEDs, the IHPs stand out as the promising still-up-and-coming choices.

In this review, as shown in Fig. 1, we first provide a comprehensive overview of the white light in WLEDs and optical properties of IHPs, with the key factors to evaluate the performance of WLEDs being also summarized. Then, we classify the WLEDs into two types according to their emitters, including WLEDs based on both inorganic lead and lead-free halide perovskites, respectively. The optimum strategies of both types of IHPs for photoluminescence and electroluminescence WLEDs, including coating, embedding, morphological optimization, and surface-ligand modification, are introduced and discussed synthetically. Especially, the device structures of electroluminescence WLEDs are analyzed to highlight the effects of carrier transport layers on the performance of lighting. Moreover, the luminescent mechanisms and properties of single-component white emission derived from inorganic lead-free halide perovskites with broad emission are presented. In addition to the lighting applications, with unique merits of high luminosity and low energy consumption, WLEDs based on IHPs are also considered as alternative candidates for visible light communication applications. Thus, the advances achieved in the visible light communication are proposed to demonstrate the prominent potential of WLEDs. Finally, further challenges toward enhanced performance and commercialization are included with discussions on the future perspectives.

2. WLEDS AND IHPS

As efficient lighting sources, WLEDs exhibit numerous advantages (e.g., low energy consumption, long duration, and ecofriendliness), emerging as the mainstream in the fields of lighting and displays. According to the pumped modes, WLEDs can be classified into photoluminescence and electroluminescence ones. For both types of WLEDs, the efficient white-emitting properties, which are evaluated by color rendering index (CRI), correlated color temperature (CCT), and luminous efficiency, facilitate lighting applications. The CRI is used to measure the rendering ability of a light source to reveal colors of objects in comparison to the sunlight; CCT is defined as the temperature of an ideal black-body radiator that radiates the light of a given lighting source. According to the CCT values of the white emission, the WLEDs can be classified into warm (2700–3700 K), neutral (3700–6500 K), and cold (over 6500 K) ones [8,13,23]. However, the cold white light with the dominant blue and ultraviolet components is found to harm the naked eyes of humans; as a result, the WLEDs with warm and neutral white light are recognized as good candidates of lighting and display sources. Therefore, it is essential for an

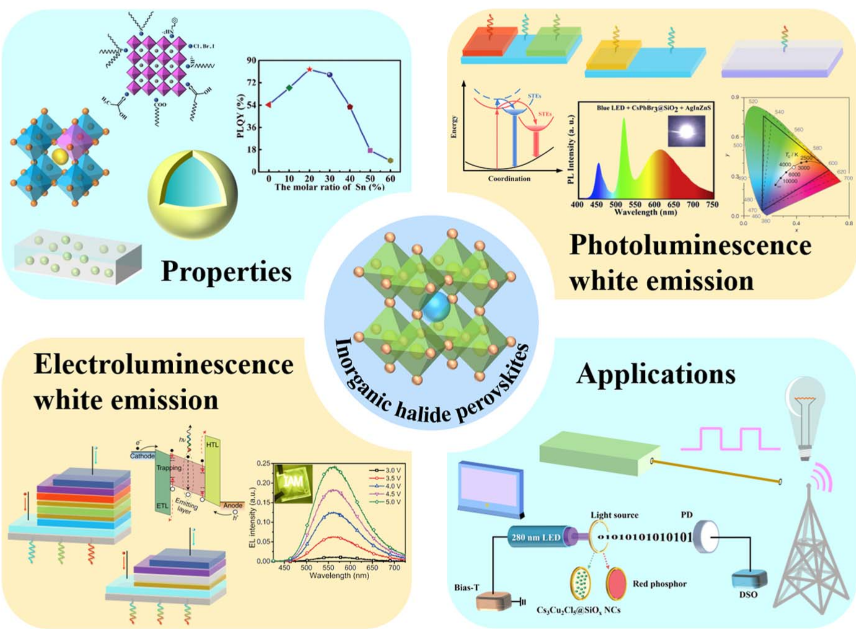

Fig. 1. Summary of the review, which includes materials, photoluminescence, and electroluminescence white emission and application of inorganic halide perovskites.

efficient WLED to possess a high CRI (near 100), a proper CCT (2700–6500 K), and a high luminous efficiency [6,24]. In terms of efficient WLEDs, their white emission originates from the combination of different colors, including the mix of yellow and blue light, as well as tricolor (red, green, and blue) light. For photoluminescence WLEDs, the yellow and tricolor components are usually derived from emitting materials, which are pumped by blue or ultraviolet (UV) chips [6]. Similarly, the electroluminescence WLEDs are accompanied by fabricating electrically driven devices with emitting and carrier transport layers [25]. Besides, the novel white emitters with broad luminescent spectra are proposed to implement WLEDs, which are of great interest for single-component white light [8,13]. As described above, the performance of WLEDs considerably depends on the optical properties of luminescent materials. Among all the bright emitters, IHPs have shown distinct advantages due to their stable perovskite-type structures and prominent optoelectronic properties.

Owing to the fascinating properties, such as high PLQYs, tunable emission, and excellent absorption, $CsPbX_3$ (X = Cl, Br, I), one of the typical known IHPs, has emerged as the dream materials for optoelectronic applications [26,27]. Besides, the studies of IHP nanocrystals have also brought new opportunities and challenges to exploit quantum confinement effects. Thus, IHP nanocrystals with size-tunable emission and high PLQYs have gained great interest in LED-related applications. Apart from IHP nanocrystals, IHP single crystals with a low defect density and controllable surface morphologies can facilitate the radiative recombination of excitons, enhancing their luminescent efficiency [28–30]. Moreover, $CsPbX_3$ perovskites feature three-dimensional structures with corner-sharing lead-halide octahedra isolated by Cs^+ ions, rendering them chemically stable. The optical properties of $CsPbX_3$ are attributed to the basic units of lead-halide octahedra. The conduction band minimum (CBM) and valence band maximum (VBM) of those IHPs originate from the antibonding orbits of lead and halide ions, in which the defect levels locate in bands [31]. It endows IHPs with outstanding abilities to tolerate defects and merits of efficient luminescence [32]. Besides, benefiting from the dependence of CBM and VBM energy levels on orbits of halide ions, the tunability of the bandgap of IHPs can be achieved through the change of halide components, leading to tunable emission. More importantly, the solution processability of IHPs without the requirement of a high temperature and a high vacuum makes it possible to deposit them over a large area while maintaining a low cost. With the abovementioned striking properties, IHPs are considered as promising candidates for efficient WLEDs in lighting applications.

3. PHOTOLUMINESCENCE WLEDS OF IHPS

A. Photoluminescence WLEDs of $CsPbX_3$

Owing to their feasible fabrication and high luminous efficiency, photoluminescence WLEDs are popular and commercialized in applications of lighting especially in recent years. Typically, photoluminescence WLEDs based on IHPs are fabricated from IHP emitters and blue/UV chips. However, $CsPbX_3$ have a small full width at half-maximum (FWHM) of emissive spectra, making them unable to achieve high-performance WLEDs with broadband emissions using a single-component $CsPbX_3$. To overcome such an issue in $CsPbX_3$ WLEDs, other emitters with complementary spectra should be added to broaden the emission [33–41]. Benefiting from the tunable emission of $CsPbX_3$, $CsPbX_3$ with different halides could serve as emitters together to form broad emission [42–44]. Among various methods to prepare $CsPbX_3$ nanocrystals, a hot-injection method evolved from the preparation of CdSe and PbS semiconductor nanocrystals is promoted [45–47]. The reaction temperature and solvent polarity during the hot-injection process were previously reported to affect the sizes and morphologies of $CsPbX_3$ nanocrystals [48,49]. It is found that high temperature and a low-polarity solvent favor nucleation and growth of $CsPbX_3$ nanocrystals, resulting in nanocrystals with uniform morphologies and high PLQYs [50]. Besides, as shown in Figs. 2(a) and 2(b), the $CsPbX_3$ nanocrystals with different sizes and halides show tunable luminescent spectra from 410 to 700 nm, covering the entire visible light region. Do *et al.* studied $CsPbX_3$ with different halide ions and ratios via the hot-injection method, with cyan $CsPb(Br_{0.75}Cl_{0.25})_3$, green $CsPbBr_3$, yellow $CsPb(Br_{0.65}I_{0.35})_3$, orange $CsPb(Br_{0.5}I_{0.5})_3$, and red $CsPb(Br_{0.35}I_{0.65})_3$ nanocrystals being synthesized through the control of halide ratios and reaction temperature [53]. By putting IHP nanocrystal films on commercial InGaN chips, Commission International de I'Eclairage (CIE) coordinates can be obtained, demonstrating the potential in pure-color display and white lighting with a large gamut.

Wang *et al.* proposed a polar-solvent-controlled ionization (PCI) method to prepare $CsPbX_3$ nanocrystals with different halide components by mixing the cesium and lead/halide precursors directly at room temperature [54]. WLEDs were then fabricated by casting red and green $CsPbX_3$ on blue GaN chips, exhibiting a CIE coordinate of (0.31, 0.34), very close to the standard CIE coordinate of (0.33, 0.33) for white light. Zeng *et al.* reported a room-temperature solution strategy to prepare $CsPbX_3$ nanocrystals [51]. The precursors with Cs^+, Pb^{2+}, and X^- are added into the nonpolar solvents, facilitating the supersaturated recrystallization of $CsPbX_3$ perovskites. When changing the ratios of halide precursors, $CsPbX_3$ with different X^- ions can be obtained at room temperature. The PLQYs and PL peaks of the obtained $CsPbClBr_2$, $CsPbBr_3$, and $CsPbBr_{1.2}I_{1.8}$ are 70% and 478 nm (blue), 95% and 513 nm (green), and 80% and 628 nm (red), respectively. The $CsPbBr_3$ and $CsPbBr_{1.2}I_{1.8}$ were dispersed into a PMMA (polymethyl methacrylate)/chloroform solution and then coated on blue chips with a PL center of 460 nm to achieve WLEDs. By changing the component ratios of green and red perovskites deposited on the blue chips, the spectra of WLEDs can be tuned, resulting in a tunable CCT in the range from 2500 to 11,500 K, as shown in Fig. 2(c).

In addition, other emitters are also combined with $CsPbX_3$ perovskites to realize white emission. Rare-earth phosphors are usually utilized in commercial WLEDs due to their broad emission and high stability, and are hence considered as suitable candidates to be mixed with $CsPbX_3$ perovskites to emit white light. Wang *et al.* excited the blend of red-emitting $CsPbBrI_2$

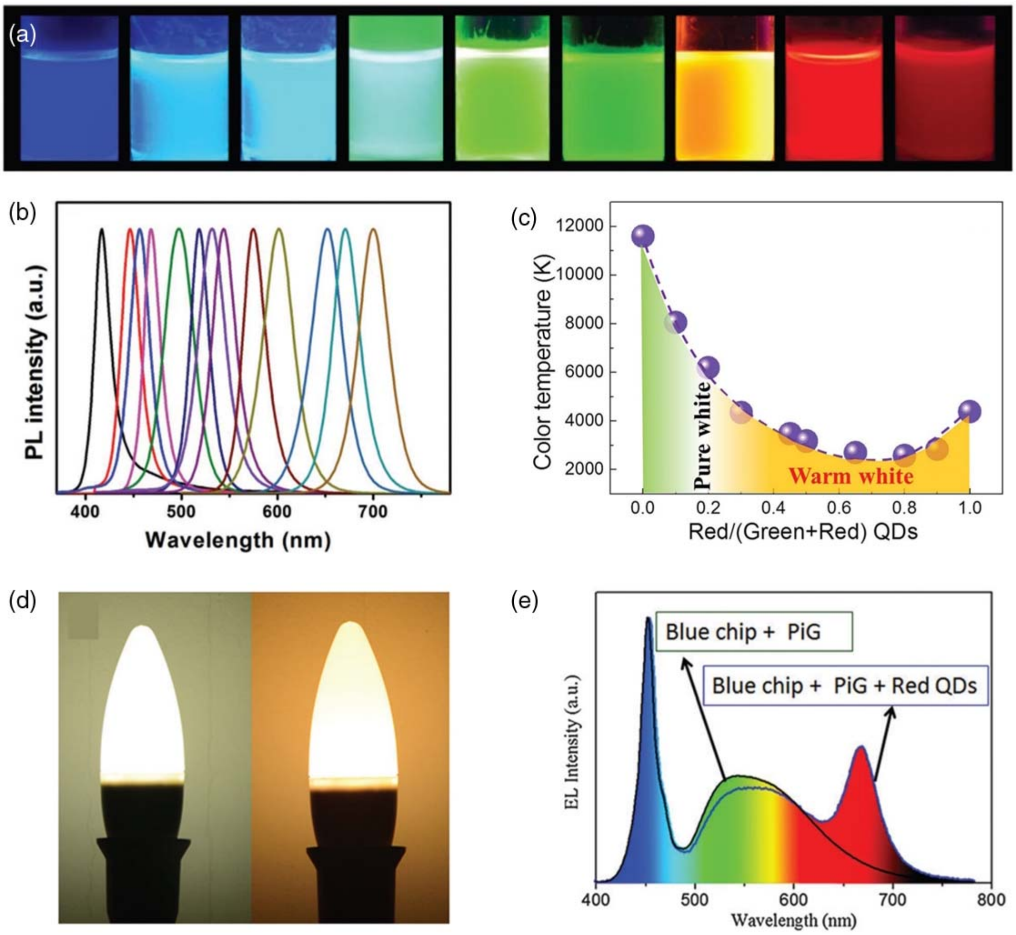

Fig. 2. (a) Photographs of $CsPbX_3$ colloidal solution in toluene under 365-nm UV irradiation. (b) PL spectra of $CsPbX_3$ nanocrystals with varied halide ions. Reproduced with permission [50]. Copyright 2016, Wiley-VCH GmbH. (c) CCT values of WLEDs as a function of component ratios of green and red perovskites. Reproduced with permission [51]. Copyright 2016, Wiley-VCH GmbH. (d) Photographs and (e) EL spectra of WLEDs with and without red-emitting $CsPbBrI_2$ nanocrystals. Reproduced with permission [52]. Copyright 2016, Royal Society of Chemistry.

nanocrystals with a yellow Ce^{3+}:YAG (yttrium aluminate garnet) phosphors glass (PiG) by blue chips, constructing IHPs/phosphors-based WLEDs, as shown in Fig. 2(d) [52]. The spectra of the WLEDs present broad emission with three luminescent peaks, corresponding to the emission of perovskites, phosphors, and blue chips, respectively [Fig. 2(e)]. The WLEDs exhibit a proper CCT of 5907 K, a high CRI of 90, and a high luminous efficiency of 58 lm/W, implying their efficient performance in lighting. Tu *et al.* fabricated WLEDs by coating $CsPbBr_3$ nanocrystals as well as red and blue phosphors on UV chips, resulting in bright white light emission with a CIE coordinate of (0.394, 0.384), a CRI of 85, and a CCT of 4026 K [55]. These obtained values are found to correspond to those of efficient WLEDs and vary slightly with the increase of the device-driving current.

However, due to the thermal instability, the luminescent intensity of $CsPbX_3$ seems to decrease when operating on blue or UV chips due to the heat release. This creates problems even in the case of WLEDs at high driving voltages for a long period. Besides, the so-called "wash" process at the end of the $CsPbX_3$ preparation is found to aggravate the surface of perovskites, especially for nanocrystals, which may increase the surface traps and defects in $CsPbX_3$, resulting in PL quenching of luminescence. Thus, strategies are required to suppress the surface defects as well as enhance the stability and luminescent properties of $CsPbX_3$ perovskites.

The surface of $CsPbX_3$ perovskites was previously reported to be fulfilled with traps and defects, including Cs^+ vacancies, Br^- vacancies, and Pb^{2+} interstitial atoms [56,57]. Thus, alkali ions, halide ions, and organic groups are typically used as the termination to decrease the surface traps [58]. For example, Wang *et al.* introduced KBr to passivate the alkali and halide vacuums on the $CsPbBr_3$ surface, leading to a high PLQY of 87% and an enhanced thermal stability [59]. The passivation effect of KBr on the surface traps is shown in Fig. 3(a). The blue KBr-passivated $CsPbBr_3$ nanoplatelets, green $CsPbBr_3$, and red $CsPbBr_{1.5}I_{1.5}$ nanocrystals are then excited by UV chips to fabricate WLEDs, showing bright white light emission with a CIE coordinate of (0.33, 0.34) and 123% of the NTSC (National Television Standards Committee) standard, suggesting an excellent white emission and a large color gamut. Xia *et al.* added ZnX_2 precursors into the as-prepared $CsPbX_3$ nanocrystals/

hexane solution to conduct a postsynthetic surface treatment [60]. Figure 3(b) shows high-resolution transmission electron microscopy (HRTEM) images of both pristine and treated $CsPbX_3$ nanocrystals. Clearly, pristine $CsPbX_3$ nanocrystals show "black dots" on the surface of nanocrystals, corresponding to PbX_2 and lead (Pb_0). The instable structure of perovskites is considered mainly caused by the defects and traps on the surface of $CsPbX_3$ nanocrystals. Under electron beam irradiation and heat/water treatment, the nanoscale structures of perovskites, i.e., octahedrons, may decompose into PbX_2 and Pb^0 due to the existence of defects and traps. In comparison, the postsynthetic treatment of ZnX_2 enables the suppression of surface defects and traps in $CsPbX_3$ nanocrystals, leading to a removal of the black dots. Figure 3(c) demonstrates the enhancement of the PL intensity for ZnX_2-treated $CsPbX_3$ nanocrystals, showing an increased PLQY of $CsPbCl_3$, $CsPbBr_3$, and $CsPbI_3$ from 4%, 58%, and 63% to 86%, 93%, and 95%, respectively. Moreover, by casting red $K_2SiF_6:Mn^{4+}$ (KSF) and green $ZnBr_2$-treated $CsPbBr_3$ on blue chips, WLEDs were also demonstrated by the authors, exhibiting a high luminous efficiency of 98 lm/W and a CIE coordinate of (0.32, 0.30). Similarly, $BaBr_2$, guanidinium bromide (GABr), and $Pb(SCN)_2$ were also introduced into $CsPbX_3$ perovskites, facilitating an improvement of both optical properties and stability in 2021 [63–65].

It is well known that organic ligands on the $CsPbX_3$ surface play an important role in the passivation of surface defects and dispersion of colloidal nanocrystals. But the conventional oleic acid (OA) and oleylamine (OAm) ligands seem to fall down from the $CsPbX_3$ surface because of their long alkyl chains. To solve such an issue, organic ligands with shorter chains and branches, as well as bounding atoms, are used to replace OA/OAm. Shi *et al*. proposed olive acid to replace OA as the surface ligands in $CsPbX_3$ because of its multiple bound points [66]. During the hot-injection preparation process, the utilization of olive acid as surface ligands is conducive to the nucleation and growth of $CsPbX_3$ nanocrystals, resulting in an increased PLQY. The blue chips are used to optically pump the combination of green $CsPbBr_3$ and red KSF phosphors, emitting white light with a CCT of 4754 K, a CRI of 85,

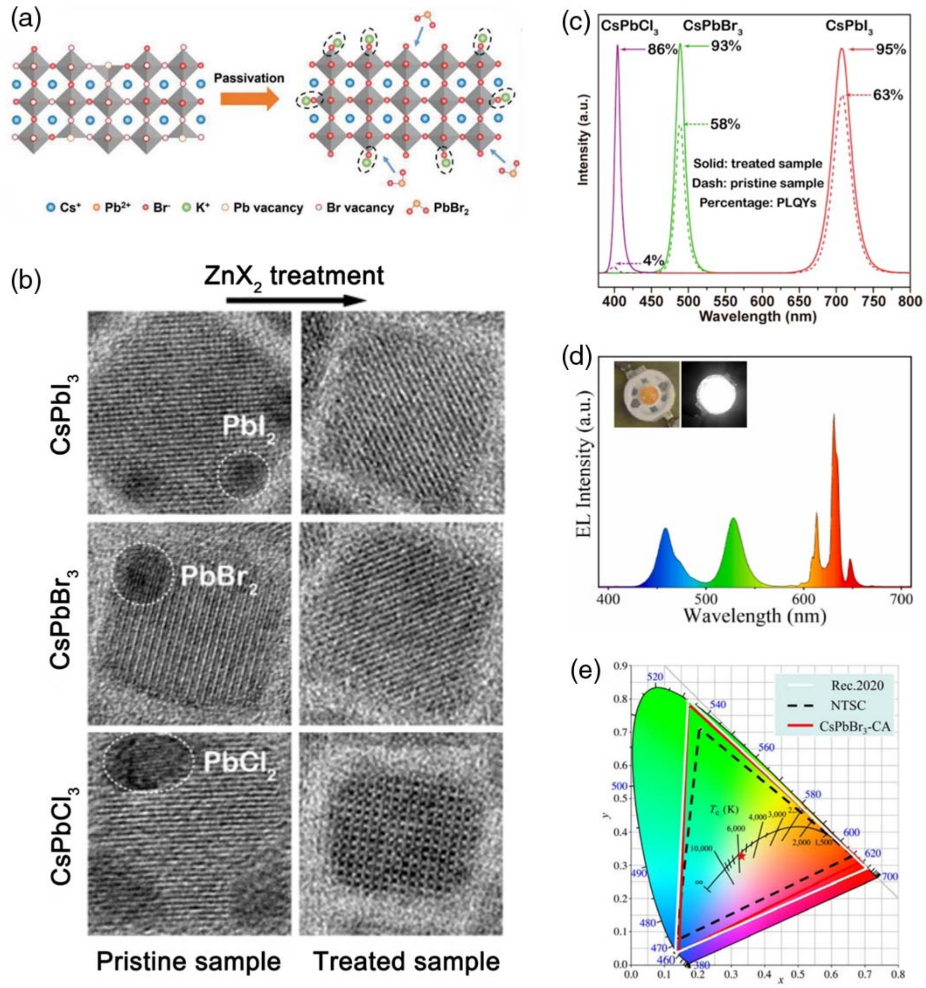

Fig. 3. (a) Representative scheme of the surface passivation of $CsPbBr_3$ nanocrystals from KBr. Reproduced with permission [59]. Copyright 2021, Wiley-VCH GmbH. (b) HRTEM images and (c) variation of PL spectra of $CsPbCl_3$, $CsPbBr_3$, and $CsPbI_3$ with ZnX_2 treatment. Reproduced with permission [60]. Copyright 2018, American Chemical Society Publications. (d) EL spectrum of WLEDs based on $CsPbBr_3$ and KSF phosphors. Reproduced with permission [61]. Copyright 2021, Elsevier Publishing Group. (e) CIE coordinates and the color gamut of WLEDs based on $CsPbBr_3$ and KSF phosphors. Reproduced with permission [62]. Copyright 2021, Springer Nature Group.

and a luminous efficiency of 46 lm/W. As a quaternary alkylammonium ligand, didodecyldimethylammonium bromide (DDAB) was proposed to passivate the surface traps of $CsPbBr_3$ nanocrystals at room temperature by Gao *et al.* [61]. With the assistance of organic acids with different chain lengths, the morphologies of $CsPbBr_3$ nanocrystals can be controlled. Importantly, the treated $CsPbBr_3$ nanocrystals show a near-unity PLQY with single radiative decay curves, suggesting reduced surface defects as a result of the effect passivation by DDAB and organic acids. The WLEDs based on the DDAB-passivated $CsPbBr_3$ show typical emissive spectra, in which the blue, green, and red emission originates from blue chips, $CsPbBr_3$, and KSF phosphors, as shown in Fig. 3(d). The CIE coordinate and the luminous efficiency of the WLEDs are (0.330, 0.329) and 12.45 lm/W, respectively, demonstrating efficient and standard white emission. Furthermore, Jing *et al.* reported a double-terminal 4, 4′-Azobis(4-cyanovaleric) acid (CA) as surface ligands bonding in $CsPbBr_3$ nanocrystals at room temperature in 2021 [62]. Owing to the strong bonding energy of CA ligands, the trap density on the surface of the $CsPbBr_3$ nanocrystals is found to reduce, leading to a high PLQY of 72% and excellent stability against heat, light, and water. The WLEDs with a CIE coordinate of (0.33, 0.33) are fabricated by coating green CA–$CsPbBr_3$ and red KSF phosphors on 460-nm blue chips, exhibiting a CCT of 5569 K, a luminous efficiency of 18.9 lm/W, and a large gamut of 126% NTSC standard and 92% Rec. 2020 standard [Fig. 3(e)].

Apart from the surface modification, coating is another effective strategy to passivate surface defects of $CsPbX_3$ perovskites and prevent them from heat, water, and polar solvents [67–69]. The coating layers, which seem as "shells" on the $CsPbX_3$, should be robust, stable, and processible. As a stable matrix, PMMA has been reported to coat and embed $CsPbX_3$ perovskites because of its good processability and low cost [70]. However, the high oxygen diffusion coefficient (3.3×10^{-9} $cm^2\,s^{-1}$ at 22°C) of PMMA may cause photo-oxygen, thus hindering the UV stability of $CsPbX_3$. Actually, among the coating materials, metal inorganics are regarded as a good candidate to coat $CsPbX_3$ perovskites. Recently, various metal inorganics, such as SiO_2, TiO_2, Al_2O_3, ZrO_2, and Si_xN_y, have been utilized to coat $CsPbX_3$ perovskites with facile methods, including physical deposition and chemical hydrolysis [71–81]. In 2016, Yu *et al.* coated $CsPbX_3$ nanocrystals with silica for the first time by adding (3-aminopropyl)triethoxysilane (APTES) into the as-prepared $CsPbX_3$ nanocrystals [82]. The addition of APTES can benefit the dissolving of PbX_2 and its silyl ether groups, enabling cross-link to cover the nanocrystals and forming a nanocrystal/silica monolith. When the nanocrystals/APTES dispersed solution is open to the air, the APTES may absorb water molecules in air and then hydrolyze to silanol (SiOH) gradually, eventually forming silica on the surface of the nanocrystals. The coated silica is found to passivate the surface defects of nanocrystals, resulting in a stabilization of colloidal $CsPbX_3$ nanocrystals and an enhanced PLQY. Importantly, the air stability of coated $CsPbX_3$ nanocrystals is also improved, implying a key role of the silica coating in the performance optimization. The coated $CsPbBr_3$ and $CsPb(Br,I)_3$ perovskites were then combined with blue chips to fabricate WLEDs, showing a CIE coordinate of (0.33, 0.33) and a high luminous efficiency of 61.2 lm/W due to the increased PLQY by the coating.

However, due to the fast hydrolysis rate of APTES, the obtained silica is regarded as a matrix to embed $CsPbX_3$ nanocrystals, resulting in nonuniform thin films by spin-coating or dip-coating. Zang *et al.* reported a controllable one-step *in situ* method to synthesize $CsPbBr_3$ nanocrystals coated with silica (SiO_2) at room temperature [83]. As shown in Fig. 4(a), the precursor solution of $CsPbBr_3$ nanocrystals is injected into toluene containing the coating precursor of APTES for the rapid growth of colloidal $CsPbBr_3$ nanocrystals. In the meantime, owing to the interaction between the amine groups of APTES and as-prepared nanocrystals, the hydrolysis of APTES occurs on the surface of nanocrystals, leading to the formation of coating silica layers. The whole process for the preparation of silica-coated $CsPbBr_3$ nanocrystals only takes 20 s, with the coating of uniform silica shells on nanocrystals being guaranteed by the amount control of APTES. Similarly, the passivating effect of silica coating enables an enhancement of PLQY of $CsPbBr_3$ nanocrystals from 35% to 75%. Moreover, compared to intrinsic perovskites, the silica-coated $CsPbBr_3$ presents improved stability under heat (80°C) and polar solvent. The coated $CsPbBr_3$ nanocrystals were then mixed with red Ag-In-Zn-S nanocrystals as emitters in WLEDs with excitation from blue chips, showing an excellent lighting performance, including a CIE coordinate of (0.404, 0.411), a high CRI of 91, a proper CCT of 3689 K, and a high luminous efficiency of 40.6 lm/W.

Apart from APTES, other silica precursors with slower hydrolysis rates were also proposed to coat $CsPbX_3$ perovskites. For example, Liu *et al.* used tetraethoxysilane (TEOS) as the precursor to coat $CsPbBr_3$ nanocrystals, where the hydrophobic and multibranched trioctylphosphine oxide (TOPO) was introduced to suppress the hydrolysis of TEOS [84]. Figure 4(b) presents the obtained monodispersed $CsPbBr_3$@ silica nanocrystals with a core-shell structure. The coated nanocrystals demonstrate a high PLQY of 87% with negligible changes of PL intensity at a high heating temperature of 120°C. The passivation of $CsPbBr_3$ induced by the coating may not affect the PL spectra but instead increase the PL decay time, as shown in Figs. 4(c) and 4(d). Besides, the robust silica shells can efficiently block the exchange of anions among colloidal nanocrystals with different halides, maintaining their original optical properties. WLEDs were fabricated by casting the green $CsPbBr_3$@ silica and red $CsPbBr_{0.6}I_{2.4}$@ silica nanocrystals on blue chips. The EL spectra with three stable luminescent peaks are observed in WLEDs driven at increased voltages, showing the negligible halide exchanges even under high voltages.

Chen *et al.* further researched the stability improvement of $CsPbX_3$@ silica nanocrystals under UV, water, and heat [85]. Owing to the prominent protective role of robust silica shells, the PL of $CsPbX_3$@ silica perovskites can maintain as high as 80% of their initial values after UV exposure and water soaking for 4000 and 3000 h, respectively. Figure 4(e) shows the variety of PL intensity of $CsPbX_3$@ silica perovskites during thermal

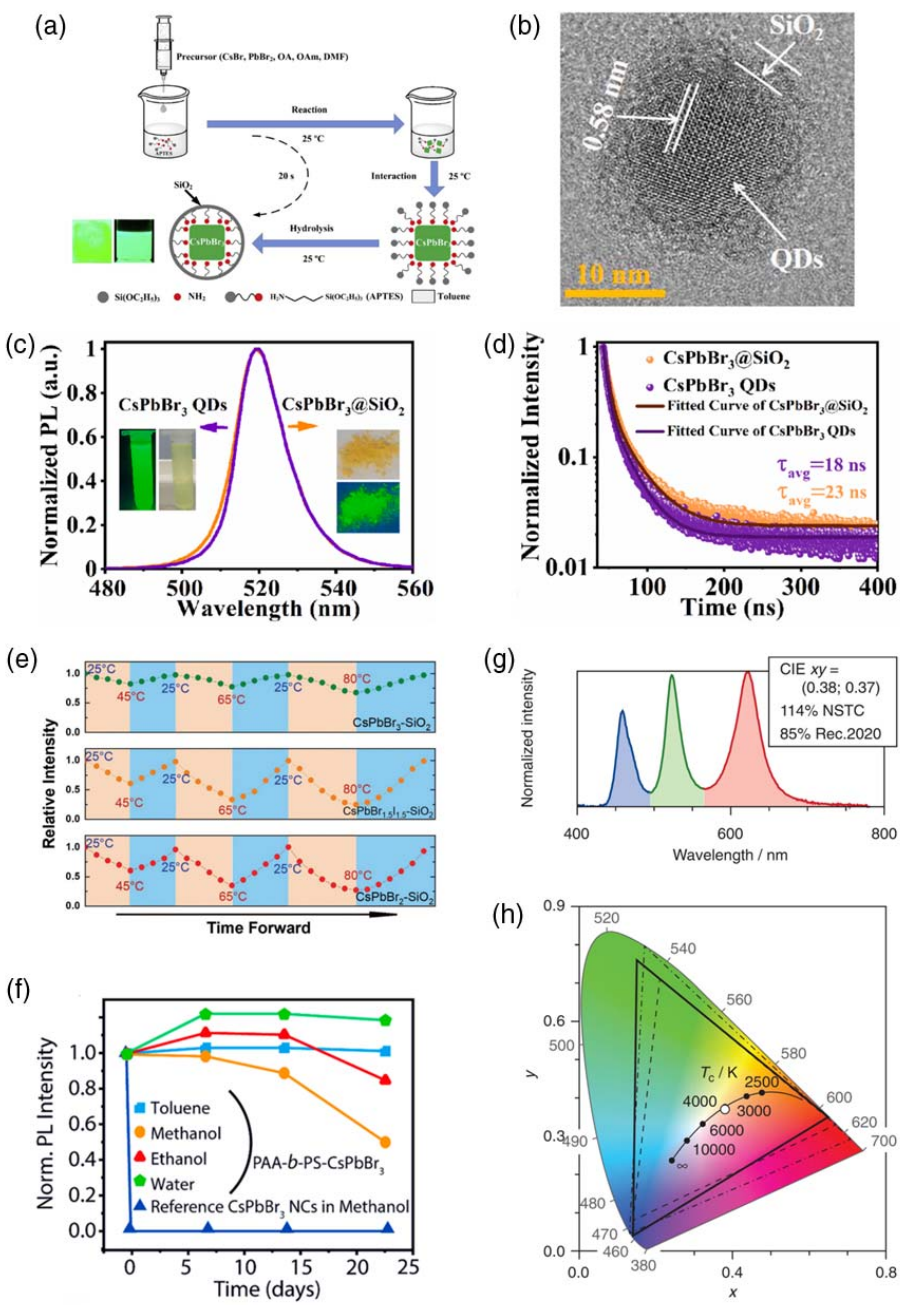

Fig. 4. (a) Schematic showing the process for coating $CsPbBr_3$ nanocrystals at room temperature. Reproduced with permission [83]. Copyright 2020, Elsevier Publishing Group. (b) HRTEM image of silica-coating $CsPbBr_3$ nanocrystals. Variety of (c) PL spectra and (d) PL decay curves of intrinsic and coated $CsPbBr_3$ perovskites. Reproduced with permission [84]. Copyright 2021, Elsevier Publishing Group. (e) Changes of PL intensity of coated $CsPbBr_3$, $CsPbBr_{1.5}I_{1.5}$, and $CsPbBrI_2$ perovskites during thermal cycling tests. Reproduced with permission [85]. Copyright 2021, Royal Society of Chemistry. (f) Stability of PAA-*b*-PS-coating $CsPbBr_3$ nanocrystals in toluene, methanol, ethanol, and water. Reproduced with permission [86]. Copyright 2021, American Chemical Society Publications. (g) EL spectrum and (h) CIE coordinate of WLEDs based on $CsPbBr_3$ and red $CsPb(Br_{0.5}I_{0.5})_3$ nanocrystals embedded in a zeolite-Y matrix. Reproduced with permission [87]. Copyright 2017, Wiley-VCH GmbH.

cycling tests, suggesting that the silica coating may suppress the thermal quenching of $CsPbBr_3$@ silica. However, with the increase of iodine ratios, the protective effects of silica at a higher temperature may not work well, as caused by the occurrences of phase changes. By exciting the mix of coated $CsPbBr_{1.5}Cl_{1.5}$, $CsPbBr_3$, and $CsPbBrI_2$ perovskites, white light with a CIE coordinate of (0.334, 0.351) and a CCT of 5433 K is exhibited. Zhang *et al.* synthesized $CsPbX_3$/oxide Janus nanocrystals by combining a water-triggered transformation process with a hydrolysis method [88]. Although the silica may not cover the entire surface of nanocrystals, the coating can improve the stability against both UV irradiation and water. In addition, hydrophobic polymers were used to coat $CsPbX_3$ perovskites, facilitating the water-resistant performance. Manna *et al.* reported a facile strategy to coat $CsPbX_3$ nanocrystals with poly(acrylic acid)-block-poly(styrene) (PAA-*b*-PS), followed by an absorption of long-chain (acrylic acid)-block-poly(styrene) molecules and an aggregation of PAA-*b*-PS micelles [86]. As shown in Fig. 4(f), the final PAA-*b*-PS would efficiently encapsulate the nanocrystals, leading to the stability enhancement under not only water but also polar solvents, including methanol, ethanol, and toluene. Rogach *et al.* introduced polyhedral oligomeric silsesquioxane to encapsulate the $CsPbBr_3$ perovskites, which were then combined with red phosphors to implement WLEDs, showing a series of excellent lighting properties, including a CIE coordinate of (0.349, 0.383), a CRI of 91, and a luminous intensity of 14.1 lm/W [89].

Embedding $CsPbX_3$ in a robust and stable matrix is another strategy to improve the optical performance and stability of inorganic perovskites [90]. The existence of interspaces is essential for the embedding candidates, which can promote the crystallization of nanoscale and microscale $CsPbX_3$ as well as accommodate them tightly [91–99]. In 2016, Liu *et al.* embedded the $CsPbX_3$ nanocrystals onto mesoporous silica particles with pore sizes of approximately 12–15 nm [100]. The pore sizes of the mesoporous silica are similar to the size of nanocrystals, enabling embedding of nanocrystals on the mesoporous silica particles. As a result, the significant enhancement of both PLQY and the stability of $CsPbX_3$ is found, inspiring the authors to apply them for white lighting. Zhang *et al.* reported a two-step method to prepare embedded $CsPbX_3$ in zeolite-Y-involved synthesis precursors, in which the as-prepared $CsPbX_3$ nanocrystals were encapsulated in the inner of the zeolite-Y matrix [87]. The embedded green $CsPbBr_3$ and red $CsPb(Br_{0.5}I_{0.5})_3$ nanocrystals were then mixed and excited by InGaN blue chips to fabricate WLEDs, showing a high performance with a CIE coordinate of (0.38, 0.37) and a CCT of 3876 K [Fig. 4(g)]. Moreover, the WLEDs present a large color gamut, covering 114% and 85% of the NTSC and Rec.2020 gamut, respectively, as shown in Fig. 4(h). Similarly, the $CsPbX_3$ perovskites were also reported to be embedded into amorphous glass [101–107] and polymer matrixes [108–118] to achieve high-performance WLEDs with efficient and stable emission.

On the other hand, as a typical semiconductor, the properties of $CsPbX_3$ perovskites can be modulated by incorporating dopants into them [119–122]. It has been found that the dopants may passivate the surface defects of $CsPbX_3$ perovskites, resulting in a further increase of luminous efficiency and improvement of stability for WLEDs [123–127]. Moreover, the doping has been certified as an effective strategy to enhance the CRI of WLEDs based on $CsPbX_3$ perovskites by introducing novel luminescent peaks, which would also compensate for the vacant regions of visible light and reduce the use of rare-earth phosphors in WLEDs. For example, Lee *et al.* and Wang *et al.* introduced Zn^{2+} and Fe^{3+} into $CsPbX_3$ nanocrystals, respectively, in which both ions were found to locate on the surface of nanocrystals [128,129]. As a result, the doped $CsPbX_3$ nanocrystals show higher PL intensity due to the passivating effects of dopant ions. In contrast, the incorporation of dopants into the inner of perovskites may change their energy-band structures and introduce novel energy levels, leading to the shifts of the original PL spectra and appearance of additional PL peaks [130,131]. Zhang *et al.* doped neodymium ions (Nd^{3+}) into $CsPbBr_3$ nanocrystals at room temperature, resulting in a shift of PL spectra to higher energy with the increase of Nd^{3+} amounts, as shown in Fig. 5(a) [132]. Such a PL shift from green to blue may be related to the tunable energy bandgap induced by the doping, as suggested by the calculated results. Besides, the doping can increase the exciton binding energy of perovskites, enhancing the PLQY of Nd^{3+}-doped $CsPbBr_3$ to ~90%. By mixing the green-doped $CsPbBr_3$ and other $CsPbX_3$, WLEDs with a CIE coordinate of (0.34, 0.33) and a CCT of 5310 K were achieved by them as well. Zang *et al.* proposed a facile antisolvent method to incorporate Sn^{2+} ions into $CsPbBr_3$ nanocrystals without using the toxic toluene [133]. With the increase of Sn^{2+} doping concentration, a slight shift of PL spectra with an obvious change of PLQY was found, showing a maximum PLQY of 82.77%. In addition, as shown in Figs. 5(b) and 5(c), the PL intensity of intrinsic $CsPbBr_3$ nanocrystals reduces to 14% after heating at 80°C for 105 min, while for doped $CsPbBr_3$, PL intensity as high as 93% of its initial value is maintained, revealing the significant enhancement of the thermal stability for Sn^{2+}-doped nanocrystals. WLEDs based on the Sn^{2+}-doped nanocrystals were then fabricated by combining them with red Ag-In-Zn-S nanocrystals, followed by casting both nanocrystals on blue chips. The as-fabricated WLEDs show excellent lighting performance, including a CRI of 89, a CCT of 3954 K, and a high luminous efficiency of 43.2 lm/W, implying the importance of doping for efficient WLEDs.

Among the dopants in $CsPbX_3$ perovskites, Mn^{2+} is regarded as a prominent candidate for the application of WLEDs, because the Mn^{2+}-doped perovskites feature novel and broad orange emission with the PL spectra at about 600 nm [136–141]. Chen *et al.* investigated the optical properties of Mn^{2+}-doped $CsPbX_3$ with various Br^-/Cl^- ratios [134]. As shown in Fig. 5(d), orange emission with an increased emissive intensity is clearly seen with the reduction of Br^-/Cl^- ratios in $CsPb(Br/Cl)_3$, mainly due to the efficient energy transfer between CBM of $CsPb(Br/Cl)_3$ and Mn^{2+} levels contributed by the larger energy differences. Alternatively, Jung *et al.* incorporated various amounts of Mn^{2+} precursors to prepare doped $CsPbCl_3$ nanocrystals, showing an orange emission with a high PLQY of 26.1% and an FWHM of 92 nm [142]. Tang *et al.* doped $CsPb(Br/Cl)_3$ nanocrystals with Mn^{2+} and then coated them with silica, resulting in a PL peak at 607 nm with a high PLQY of 50.5% and excellent thermal stability of the as-prepared nanocrystals [135]. Thanks to the broad and efficient orange emission induced from Mn^{2+} doping, the WLEDs obtained by exciting the combination of the Mn^{2+}-doped $CsPb(Br/Cl)_3$ and green $CsPbBr_3$ nanocrystals with UV chips display a high CRI of 91 and a high luminous efficiency of 68.4 lm/W. As shown in Figs. 4(e) and 4(f), while the EL intensity of the WLEDs increases with the increase of driving current, the thermal effect at a higher current causes the PL quenching of nanocrystals, leading to the shifts of CCT to the blue region. In addition to Mn^{2+}, rare-earth element Eu^{3+} was

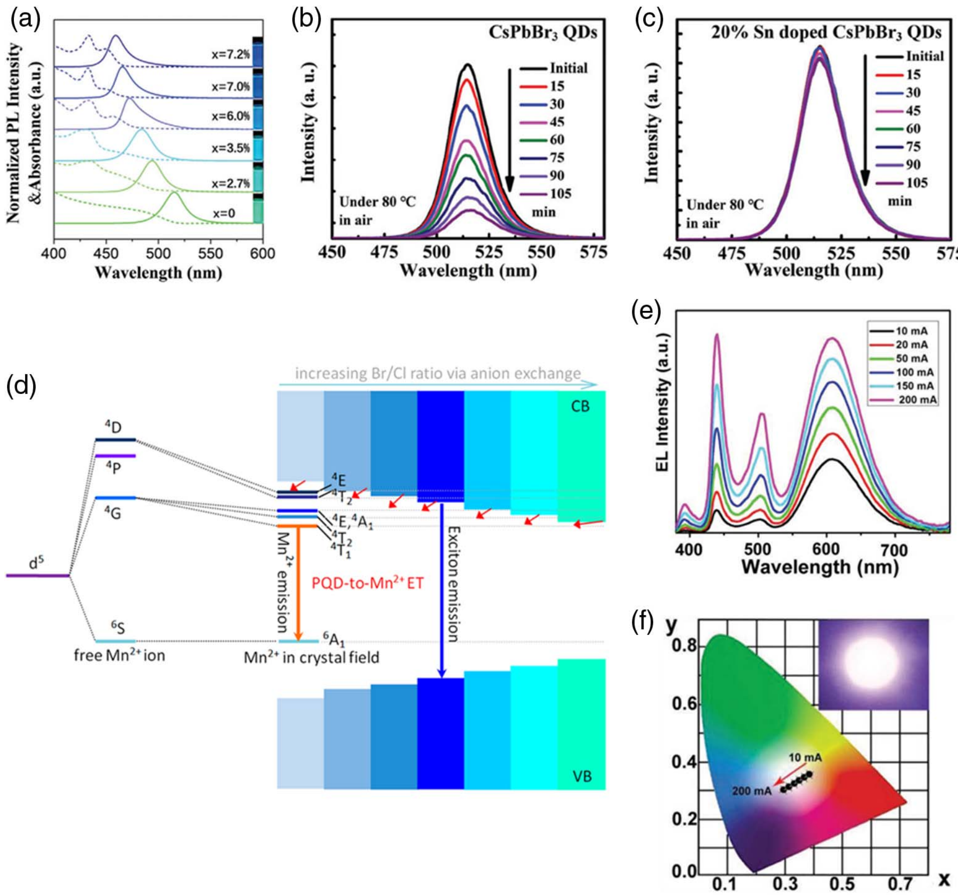

Fig. 5. (a) PL and absorption spectra of Nd^{3+}-doped $CsPbBr_3$ nanocrystals with various Nd^{3+} amounts. Reproduced with permission [132]. Copyright 2020, Wiley-VCH GmbH. PL variation of (b) intrinsic and (c) Sn-doped $CsPbBr_3$ nanocrystals heated at 80°C in air. Reproduced with permission [133]. Copyright 2021, Royal Society of Chemistry. (d) An energy level diagram of Mn^{2+} ions in $CsPb(Cl/Br)_3$ with increased Br/Cl ratios. Reproduced with permission [134]. Copyright 2017, American Chemical Society Publications. Evolution of (e) EL spectra and (f) CIE coordinates of WLEDs driven by increasing currents. Reproduced with permission [135]. Copyright 2019, Wiley-VCH GmbH.

doped into $CsPbBr_3$ nanocrystals by Zhang *et al.* [143]. Benefiting from the numerous transition energy levels in Eu^{3+}, the Eu^{3+}-doped $CsPbBr_3$ demonstrates a series of narrow PL peaks ranging from 540 to 710 nm, offering great merits for white emission.

Apart from the doping with single ions, two doping ions are incorporated into $CsPbX_3$ perovskites together (i.e., codoping) to further promote the development of $CsPbX_3$ in the WLEDs. For example, Song *et al.* codoped Ce^{3+}/Mn^{2+}, Ce^{3+}/Eu^{3+}, Ce^{3+}/Sm^{3+}, Bi^{3+}/Eu^{3+}, and Bi^{3+}/Sm^{3+} into $CsPbCl_xBr_{3-x}$ nanocrystals, respectively, achieving a PLQY as high as 75% in Ce^{3+}/Mn^{2+}-codoped $CsPbCl_xBr_{3-x}$, mainly due to the improved energy transfer from nanocrystals to Mn^{2+} assisted by Ce^{3+} [144]. Besides, the existence of Ce^{3+} ions may broaden the blue and green PL spectra of $CsPbCl_xBr_{3-x}$. By exciting the Ce^{3+}/Mn^{2+}-codoped $CsPbCl_xBr_{3-x}$ with 365-nm GaN chips, WLEDs with white emission were obtained by them, which display a CIE coordinate of (0.33, 0.23) and a CRI of 89. A similar phenomenon and similar results were also reported later by the same group and Yang *et al.*, who codoped Bi^{3+}/Mn^{2+} and Tm^{3+}/Mn^{2+} into $CsPbX_3$ perovskites, respectively, demonstrating the importance of codoping in high-quality WLEDs [145,146].

B. Photoluminescence WLEDs of Inorganic Lead-Free Halide Perovskites

Despite the fascinating characteristics and promising white lighting applications, the commercialization of $CsPbX_3$ perovskites is still hindered by the toxicity of Pb elements and the intrinsic narrow PL spectra. To overcome the toxicity and performance limitation in the lighting applications, inorganic lead-free halide perovskites are proposed to serve as emitters in WLEDs. Among all the inorganic lead-free halide perovskites, $Cs_3Cu_2X_5$ and $CsCu_2X_3$ with nontoxic copper elements have attracted wide attention due to their novel properties and outstanding potentials in WLEDs [147–149]. Hosono *et al.* synthesized $Cs_3Cu_2I_5$ single crystals as well as characterized their crystal structures and electronic configurations [150]. Figure 6(a) displays the crystal structure of $Cs_3Cu_2I_5$, which consists of zero-dimensional (0D) $[Cu_2I_5]^{3-}$ dimers and isolated Cs^+ ions; this is significantly different from $CsPbX_3$ perovskites featuring 3D corner-sharing $[PbX_6]^{4-}$ octahedra structures. Thus, compared to $CsPbX_3$ perovskites, $Cs_3Cu_2I_5$ exhibits distinguishing optical performance, including a large Stokes shift of 155 nm, a broad PL spectrum with an FWHM of ~100 nm, and a long PL decay time, as shown in Fig. 6(b). The distinguishing optical properties suggest that the PL mechanism of lead-free

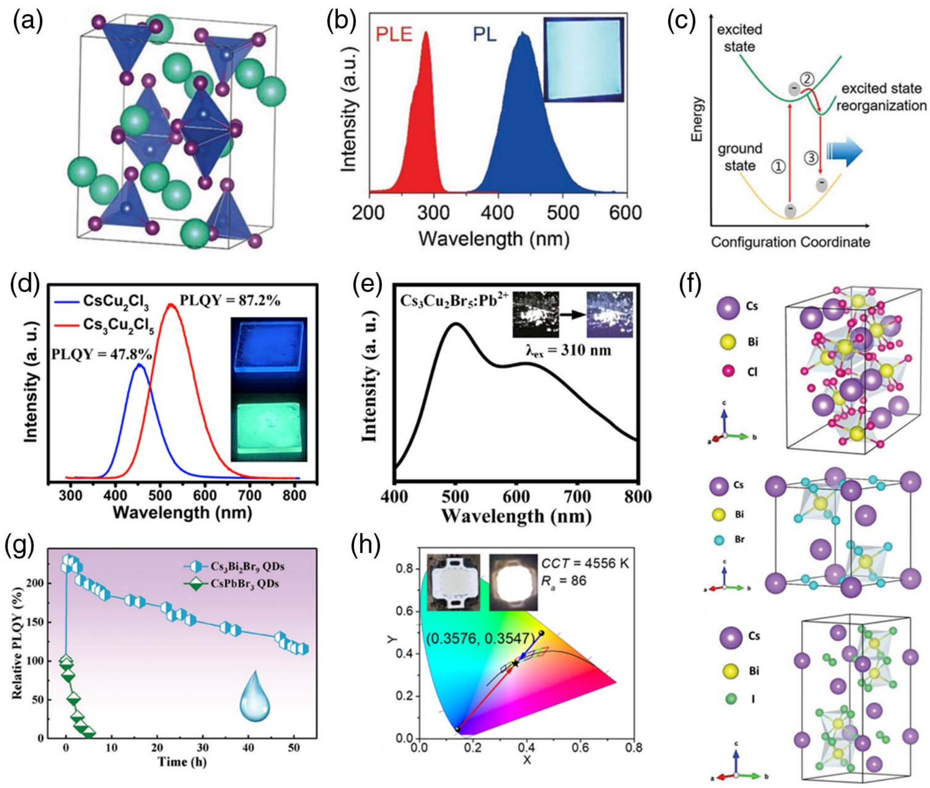

Fig. 6. (a) Schematic of the crystal structure of $Cs_3Cu_2I_5$. (b) PL and PLE spectra of $Cs_3Cu_2I_5$. (c) Schematic configuration coordinate for the excited-state reorganization in $Cs_3Cu_2I_5$. Reproduced with permission [150]. Copyright 2018, Wiley-VCH GmbH. (d) PL spectra of $Cs_3Cu_2Cl_5$ and $CsCu_2Cl_3$ prepared at 120°C and 70°C, respectively. Reproduced with permission [151]. Copyright 2021, Chinese Laser Press. (e) White PL spectra of Pb-doped $Cs_3Cu_2Br_5$ nanocrystals excited at 310 nm. Reproduced with permission [152]. Copyright 2021, Cell Press. (f) Schematics of crystal structures of $Cs_3Bi_2X_9$ (X = Cl, Br, I). Reproduced with permission [153]. Copyright 2018, Wiley-VCH GmbH. (g) Evolution of PLQY of $Cs_3Bi_2X_9$ and $CsPbBr_3$ nanocrystals after adding water. Reproduced with permission [154]. Copyright 2020, Royal Society of Chemistry. (h) CIE coordinates of WLEDs based on Sb^{3+}-doped $Cs_2InCl_5 \cdot H_2O$. Reproduced with permission [155]. Copyright 2020, American Chemical Society Publications.

$Cs_3Cu_2I_5$ may not be ascribed to the band-edge emission. Instead, the PL of $Cs_3Cu_2I_5$ is found to originate from the self-trapped excitons (STEs) emission, which results from the 0D configuration and the soft lattice of $Cs_3Cu_2I_5$. Under light excitation, the electronic configuration of $[Cu_2I_5]^{3-}$ dimers may change to the excited ones with higher energy, leading to a structural distortion of crystals; this is called as the "Jahn-Teller distortion." The existence of Jahn-Teller distortion in excited $Cs_3Cu_2I_5$ crystals can give rise to the reorganization of the excited-state structure. As a result, the excited electrons first relax to the reorganized excited state to form STEs with holes in the distorted crystals and then recombine to emit light, as shown in Fig. 6(c). Therefore, the large Stokes shift is owing to the difference between the original bandgap and the exciton energy of excited structures, while the broad emission with a long decay time can be explained by the distorted electronic structure and crystalline configuration [156]. Benefiting from the large Stokes shifts and the broad emission, the perovskites show negligible self-absorption with an increased emissive covering region, which results in the enhanced optical performance of the WLEDs. By mixing the blue $Cs_3Cu_2I_5$ with yellow $CsCu_2I_3$, the controllable white emission with a high CRI and a proper CCT value was achieved [157–159]. Furthermore, due to the broad PL spectrum of yellow $CsCu_2I_3$, Huang *et al.* utilized it to serve as emitters in WLEDs without the need for other phosphors [160]. The as-fabricated WLEDs show a CIE coordinate of (0.345, 0.364) and a CCT of 5035 K, revealing their prominent potentials in single-component WLEDs.

Zang *et al.* reported a facile hot-injection method to prepare $Cs_3Cu_2Cl_5$ and $CsCu_2Cl_3$ nanocrystals at 120°C and 70°C, respectively [151]. As shown in Fig. 6(d), the PL peaks of $Cs_3Cu_2Cl_5$ and $CsCu_2Cl_3$ nanocrystals locate at 518 and 453 nm, respectively, with the PL mechanism of them dominated by STEs. WLEDs were then fabricated by casting both crystals and red phosphors on UV chips, showing a CIE coordinate of (0.337, 0.338), a high CRI of 94, and a CCT value of 5285 K, and demonstrating the excellent potential in lighting applications. To further enhance the performance of WLEDs based on $Cs_3Cu_2X_5$ and $CsCu_2X_3$, one effective strategy is doping. By doping Nd^{3+} into the $Cs_3Cu_2I_5/CsCu_2I_3$ system, Zhong *et al.* obtained the coexistence of high-efficiency and stable $Cs_3Cu_2I_5$ and $CsCu_2I_3$ with varied ratios, which was beneficial for the achievement of WLEDs [161]. Alternatively, Zang *et al.* doped small amounts of Pb^{2+} into $Cs_3Cu_2Br_5$ nanocrystals via a hot-injection method, in which the Pb^{2+} ions act as the centers of isolated $[PbBr_6]^{4-}$ octahedra, and achieved two STEs PL originated from distorted 0D $[PbBr_6]^{4-}$ octahedra and $[Cu_2I_5]^{3-}$ dimers [152]. Figure 6(e) shows a broad blue intrinsic and red emission, enabling the formation of integrated white light by exciting the nanocrystals with 310-nm UV chips. The obtained single-component WLEDs exhibit a CCT of 5469 K, a high CRI of 98, and excellent operating stability of more than 200 h.

Apart from copper, other nontoxic elements, such as Ag^+, Bi^{3+}, and Sb^{3+}, are also used to replace Pb in perovskites to form polyhedra with halide ions [162–168]. Tang *et al.* prepared colloidal $Cs_3Bi_2X_9$ nanocrystals via adding CsX and BiX_3 into the reaction precursors [153]. As shown in Fig. 6(f), while $Cs_3Bi_2Cl_9$ possesses a monoclinic structure, both $Cs_3Bi_2Br_9$ and $Cs_3Bi_2I_9$ belong to hexagonal structures. With the variety of halide ions from Cl^- to I^-, the corresponding PL spectra are found to shift from 393 to 545 nm, exhibiting the similar PL tunability to $CsPbX_3$ perovskites. By mixing the blue $Cs_3Bi_2Br_9$ nanocrystals with yellow phosphors, WLEDs were fabricated, showing a CIE coordinate and a CCT of (0.29, 0.30) and 8477 K, respectively. Shi *et al.* reported a room-temperature water-induced strategy to prepare $Cs_3Bi_2X_9$ nanocrystals with an increased PLQY from 20.2% to 46.4%, thanks to the formation of BiOX on the surface of corresponding nanocrystals [154]. The BiOX encapsulation enables the suppression of surface defects of $Cs_3Bi_2X_9$ nanocrystals, resulting in the enhancement of optical performance, as shown in Fig. 6(g). Besides, it has been well known that intrinsic $CsPbX_3$ perovskites exhibit a poor stability in water with PL quenching because of the rapid decomposition to CsX and PbX_2. In comparison to $CsPbX_3$, the presence of BiOX on the surface of $Cs_3Bi_2X_9$ nanocrystals can work as a protection layer. As a result, the stability significantly enhanced with the PL intensity of $Cs_3Bi_2Br_9$ nanocrystals in water increases first by 130% and reduces gradually to its initial value for 52 h, as compared to a PL intensity quenching of $CsPbBr_3$ for only 5 h. The blue $Cs_3Bi_2Br_9$ nanocrystals were then mixed with yellow phosphors to construct WLEDs, resulting in a CIE coordinate of (0.321, 0.334) and improved operating stability. Further, Tang *et al.* found that the incorporation of 2.75% Bi^{3+} dopants into Cs_2SnCl_6 could increase its PLQY to 78.9% due to the strong blue emission derived from the $Bi_{Sn} + V_{Cl}$ defect complex [169]. Owing to the bright blue emission at 455 nm and the large Stokes shift of 106 nm for Bi^{3+}-doped Cs_2SnCl_6, the WLEDs based on the lead-free perovskites and yellow phosphors demonstrate excellent performance, including a CIE coordinate of (0.36, 0.37) and a CCT of 4486 K. Xia *et al.* prepared air-stable $Cs_2InCl_5 \cdot H_2O$ crystals and doped various amounts of Sb^{3+} into the crystals [155]. By replacing In^{3+} with Sb^{3+}, a small lattice deformation may occur, leading to the enhancement of absorption intensity and a red shift of the absorption edges. By exciting with 340-nm UV light, the Sb^{3+}-doped $Cs_2InCl_5 \cdot H_2O$ emits STE-dominated bright yellow light at 580 nm with a large Stokes shift of 240 nm and a high PLQY up to 95.5%. The utilization of the Sb^{3+}-doped $Cs_2InCl_5 \cdot H_2O$ crystals with blue phosphors as the emitters also enables the fabrication of the single-component WLEDs with a CIE coordinate of (0.358, 0.355), a CRI of 86, and a CCT of 4556 K, as shown in Fig. 6(h), indicating the prospective applications of the doped lead-free perovskites in white light.

Recently, lead-free double perovskites have received substantial research interest due to their tunable properties and wide applications in lighting. According to the chemical formula, the double perovskites can be divided to two main types: $A_2M^+M^{3+}X_6$ and $A_4M^{2+}M_2^{3+}X_{12}$, where the M represents the lead-free elements. In double perovskites, while the lead-free elements enable the formation of $[MX_6]$ octahedra, the configuration and structure of the octahedra may endow the double perovskites with varied dimension, crystal structures, and optoelectronic properties [170]. The broad emissive spectra of double perovskites make them possible to be employed directly as emitters in efficient WLEDs. Kuang *et al.* designed and synthesized a novel $Cs_4MnBi_2Cl_{12}$ double perovskite with a 2D layered structure, in which the inner $[BiCl_6]^{3-}$ facilitates the activation of electrons in d orbits of Mn^{2+} ions [171]. As shown in Fig. 7(a), the enhanced d–d transition in Mn^{2+} leads to an emission centered at 610 nm with a high PLQY of 25.7% and long decay time of 144 μs. The blend of $Cs_4MnBi_2Cl_{12}$ crystals with blue and green phosphors could therefore achieve efficient WLEDs with a CIE coordinate of (0.32, 0.30).

To further enhance performance of WLEDs based on double perovskites and cut the use of rare-earth phosphors, the doping and alloying strategies have been adopted by researchers to broaden the covering regions and increase the luminescent efficiency of double perovskites [176–182]. Shi *et al.* incorporated small amounts of Sb^{3+} and Bi^{3+} ions into $Cs_2NaInCl_6$, resulting in dual emission locating at 450 and 580 nm with a high PLQY of 77%, as shown in Fig. 7(b) [172]. Specifically, the broad blue emission arises from the STEs in $[SbCl_6]^{3-}$ octahedra with a small deformation, while the yellow emission is attributed to the increased deformation of the $[SbCl_6]^{3-}$ octahedra induced by the doping of Bi^{3+} ions. The presence of broad blue and yellow emission enables the white light in the Sb^{3+}/Bi^{3+}-codoped $Cs_2NaInCl_6$, illustrating the important role of doping in spectral tunability and achievement of white emission. Yella *et al.* investigated a variety of electronic structures and bandgaps of Bi^{3+}-alloyed $Cs_2AgInCl_6$ [173]. With the increase of Bi^{3+} amounts, the electronic structures of double perovskites change from direct transition to indirect transition [Fig. 7(c)], accompanying the variety of bandgap results. In addition, the emissive intensity of dual emission at ~420 nm and 570–620 nm, which corresponds to the intrinsic band-edge emission and sub-band gap emission, respectively, is found to change with the variety of Bi^{3+}-alloyed amounts, as shown in Fig. 7(d). The choice of 30% Bi^{3+}-alloyed $Cs_2AgInCl_6$ as the emitter enables the fabrication of single-component WLEDs with a CIE coordinate of (0.36, 0.35), a high CRI of 91, and a CCT of 4443 K. Tang *et al.* alloyed Na^+ ions into $Cs_2AgInCl_6$ double perovskites to break the parity-forbidden transition by manipulating the parity of the wavefunction of the self-trapped exciton, resulting in a significant increase of PLQY for the alloyed samples [174]. Furthermore, as shown in Fig. 7(e), by doping 0.04% Bi^{3+} into the optimized $Cs_2Na_{0.4}Ag_{0.6}InCl_6$, a maximum PLQY of 86.2% can be obtained, which is 3 and 4 orders of magnitude higher than that of intrinsic $Cs_2AgInCl_6$. Apart from the

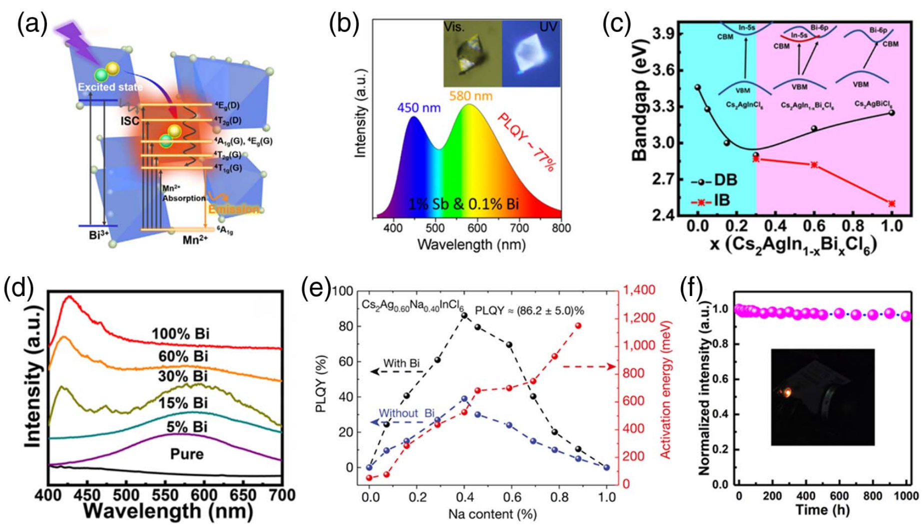

Fig. 7. (a) Energy-level diagram of $Cs_4MnBi_2Cl_{12}$. Reproduced with permission [171]. Copyright 2020, Cell Press. (b) PL spectrum of Sb^{3+}/Bi^{3+}-codoped $Cs_2NaInCl_6$. Reproduced with permission [172]. Copyright 2021, American Chemical Society Publications. (c) Estimated band gap values of $Cs_2AgIn_{1-x}Bi_xCl_6$ measured from Tauc plots for both direct and indirect transitions. (d) A variety of PL spectra of $Cs_2AgIn_{1-x}Bi_xCl_6$ perovskites. Reproduced with permission [173]. Copyright 2019, American Chemical Society Publications. (e) Activation energy and PLQYs of $Cs_2Ag_xNa_{1-x}InCl_6$. Reproduced with permission [174]. Copyright 2018, Springer Nature Group. (f) Evolution of EL intensity of WLEDs based on Bi^{3+}–$Cs_2Ag_{0.7}Na_{0.3}InCl_6$. Reproduced with permission [175]. Copyright 2020, American Chemical Society Publications.

high PLQY, the use of Bi-doped $Cs_2Na_{0.4}Ag_{0.6}InCl_6$ also enables ultrastable white emission with a CIE coordinate of (0.396, 0.448) and a CCT of 4054 K, meeting the requirement of solid-state lighting. Li *et al.* prepared Bi-doped $Cs_2Na_{0.3}Ag_{0.7}InCl_6$ double perovskites and applied them into WLEDs [175]. Owing to the broad emission of the double perovskites, the white light can be achieved by directly exciting it with UV chips. The resulted WLEDs show a CIE coordinate of (0.38, 0.44), a CCT of 4347 K, and a CRI of 87.8. Besides, as shown in Fig. 7(f), the EL intensity of the operating WLEDs maintains 90% of its initial value after 1000 h, suggesting the excellent operating stability as lighting sources. To sum up, owing to the broad emission with large Stokes shifts derived from STEs, the photoluminescence WLEDs based on lead-free perovskites exhibit excellent performance including high CRI values and prominent stability, making them great candidates in lighting applications.

4. ELECTROLUMINESCENCE WLEDS OF IHPS

Although photoluminescence WLEDs based on IHPs have been researched for years, their current efficiency, which is defined as the ratio of luminance to current, is relatively low due to the thermal relaxation and energy loss in chips. Compared to photoluminescence WLEDs, the emission of electroluminescence WLEDs originates from the direct recombination of carriers confined in the emitting layers, recognized as the efficient utilization of current and energy [170,183]. Moreover, for IHPs, their Cs^+, Rb^+, and K^+ cations with a small radius are found to exhibit increasing ion migration. In comparison, the organic cations with a large radius limit the ion migration in hybrid perovskites [184–186]. Therefore, the enhanced ion migration in IHPs facilitates the release of the Joule heat in LEDs, improving the lifetime of emitting devices. Therefore, researchers start to pay more attention on the IHP-based electroluminescence WLEDs. The emitting materials and parameters of the WLEDs based on IHPs are summarized in Table 1.

In 2017, Yang *et al.* employed the blend of $CsPbBr_xCl_{1-x}$ with poly[2-methoxy-5-(2-ethylhexyloxy)-1,4-phenylenevinylene] (MEH:PPV) as an emitting layer to construct WLEDs [187]. Figure 8(a) shows the energy band structure of the WLEDs, where the injected carriers (i.e., electrons and holes) are confined in the emitting layer. It is found that the emission of $CsPbBr_xCl_{1-x}$ and MEH:PPV locates at 470 and 560 nm, respectively. Thus, by changing the ratios of $CsPbBr_xCl_{1-x}$ and MEH:PPV in the emitting layer, WLEDs with different spectra were demonstrated with varied EL intensity of both emitters. Figure 8(b) depicts the CIE coordinates of electroluminescence devices with different ratios of $CsPbBr_xCl_{1-x}$ and MEH:PPV, with the optimum WLEDs [a corresponding CIE coordinate of (0.33, 0.34)] being achieved at a ratio of 9:1. Figure 8(c) presents the current density-voltage ($J-V$) and luminance-voltage ($L-V$) curves of the WLEDs, demonstrating that their maximum luminance reaches up ~350 cd/m^2. Choy *et al.* designed multilayer-structure electroluminescence WLEDs with cyan $CsPb(Br, Cl)_3$ and red $(CH_3CH_2CH_2NH_3)_2CsPb_2I_7$ emitters [189]. To hinder the anion exchange between $CsPb(Br, Cl)_3$ and $(CH_3CH_2CH_2NH_3)_2CsPb_2I_7$ perovskites, two organic layers were deposited between both perovskites acting as interlayers. The CIE coordinate and CCT of the WLEDs are found to be (0.32, 0.32) and ~6000 K, respectively, and the maximin external quantum efficiency (EQE) reaches 0.22%. Song *et al.* introduced Sm^{3+} ions into $CsPbCl_3$ nanocrystals and found the presence of Sm^{3+} shifts the PL to

Table 1. Summary of Emitting Materials and Key Parameters of Electroluminescence WLEDs Based on IHPs

Emitters	CIE Coordinate	CRI	CCT (K)	Luminance (cd/m^2)	EQE (%)	Ref.
$CsPb(Cl, Br)_3$/MEH:PPV	(0.33, 0.34)			350		[187]
$CsPbCl_{1.5}Br_{1.5}$/HFSO	(0.28, 0.33)			1200		[188]
$CsPb(Cl, Br)_3/PA_2CsPb_2I_7$	(0.32, 0.32)		~6000		0.22	[189]
$CsPbBr_3$/p–GaN/n–ZnO	(0.309, 0.323)			267	0.042	[190]
Mn–$CsPb(Cl, Br)_3$/red & green phosphors	(0.311, 0.326)			102	0.25	[191]
$CsPb(Cl, Br)_3$/ZnCdS/ZnS	(0.34, 0.34)	75	5153	275	0.015	[192]
$CsPbBr_{2.5}I_{0.5}/CsPbBr_3$	(0.31, 0.36)			657		[193]
Sm^{2+}–$CsPbCl_3$	(0.32, 0.31)	93		938	1.2	[194]
$CsPbX_3$/carbon QDs	(0.41, 0.44)	92	3900	140	0.06	[195]
Zn–$CsPbBr_3$/PVK	(0.356, 0.356)	71		860.9	0.22	[196]
α–$CsPbI_3$/δ–$CsPbI_3$	(0.35, 0.43)			12200	6.5	[197]
$Cs_3Cu_2I_5/CsCu_2I_3$	(0.38, 0.42)	91.6	4264	145	0.15	[198]
$CsCu_2I_3$/blue phosphors	(0.27, 0.31)		10,000			[150]
$Cs_3Cu_2I_5/CsCu_2I_3$	(0.327, 0.348)	94		352.3	0.053	[199]
$Cs_3Cu_2I_5/CsCu_2I_3$	(0.44, 0.53)		3650	1570	3.1	[200]
$Cs_2AgIn_{0.9}Bi_{0.1}Cl_6$	(0.32, 0.32)	94.5	6432	158	0.08	[201]

the range of 550–680 nm [194]. With the increase of the Sm^{3+} dopants concentration, the enhanced energy transfer from the perovskites to Sm^{3+} ions results in an increase of emissive intensity derived from Sm^{3+} and a reduction of the PL intensity of the blue emission from the intrinsic $CsPbCl_3$. At a Sm^{3+} doping percentage of 5.1% (molar ratio), the emission from perovskites and dopants exhibits similar intensity, facilitating the white emission. Consequently, it is adopted as the emissive layer in WLEDs with the structure of ITO/ZnO/PEI/Sm^{3+}– doped $CsPbCl_3$/TCTA (p-type 4, 4′, 4″-tris(carbazol-9-yl) triphenylamine)/MoO_3/Au. The single-component WLEDs display a CIE coordinate of (0.33, 0.32) and a CRI of 93, as well as a maximum luminance and an EQE of 938 cd/m^2 and 1.20%, respectively.

Zeng *et al.* studied the preparation and properties of both α and δ phases $CsPbI_3$. While α–$CsPbI_3$ can emit red light due to the band-edge mechanism, δ–$CsPbI_3$ exhibits a broad emission ranging from ~410 to ~700 nm as derived from STEs [197]. Thus, thin films with the combination of α- and δ–$CsPbI_3$ are prepared for WLEDs [Fig. 8(d)], with α–$CsPbI_3$ facilitating the carrier transport because of its high mobility and δ–$CsPbI_3$ serving as an emitter. Figure 8(e) displays a photograph of the operated WLEDs driven at 5.2 V, featuring bright and uniform white emission with a CIE coordinate of (0.35, 0.43). As shown in Fig. 8(f), the WLEDs display a typical white emissive spectrum with the broad and red emission originating from the δ- and α–$CsPbI_3$ in the blending emitting layer, respectively. Although the current density is enhanced with the increase of the driving voltages for the WLEDs due to the diode characteristics, the luminance rises and then reaches saturation, achieving a maximum luminance of 12,000 cd/m^2 under a driving voltage of 6.6 V [Fig. 8(g)]. The EQE and current efficiency of the WLEDs are found to reduce gradually as a function of current density, in which a maximum EQE and a current efficiency of 6.5% and 12.23 cd/A were achieved, respectively, as shown in Fig. 8(h).

Shi *et al.* reported a one-step method to prepare $CsCu_2I_3/Cs_3Cu_2I_5$ thin films, in which PL spectra are found to vary with different CsI/CuI ratios in the precursors, as shown in Fig. 9(a) [198]. Clearly, the increase of CuI in the precursors enables the synthesis of more yellow $CsCu_2I_3$ in the composites, facilitating the warm white emission with a CRI of 91.6 and a CCT of 4264 K. Figure 9(b) presents the EQE characteristics of the cold, standard, and warm WLEDs with CIE coordinates of (0.28, 0.29), (0.32, 0.33), and (0.38, 0.42), respectively. Similarly, the EQE of the three WLEDs rises and then reduces with the increase of driving voltages, reaching maximum EQE values of ~0.1% at driving voltages of ~7 V. Moreover, Fig. 9(c) plots a lifetime curve of the WLEDs running at 7 V, from which an operating lifetime (T_{50}, time to half of the initial luminance) of 238.5 min can be obtained. The reduction of the luminance of the WLEDs is attributed to the increase of device temperature from 37.5°C to 59.9°C during the operation at high running voltages, which generates massive joule heat. The presence of joule heat may give rise to the formation of nonradiative recombination centers in the devices, quenching their luminous performance.

In 2021, Wang *et al.* added Tween (polyethylene glycol sorbitan monooleate) into a precursor solution consisting of CsI and CuI and then spin-coated them to prepare $CsCu_2I_3/Cs_3Cu_2I_5$ thin films [200]. A grazing-incidence wide-angle X-ray scattering (GIWAXS) measurement is performed to investigate the effects of Tween on the crystallization of $CsCu_2I_3/Cs_3Cu_2I_5$ thin films. As shown in Fig. 9(d), during the spin-coating process, the signals of both $CsCu_2I_3$ and $Cs_3Cu_2I_5$ are observed at the same time of 33 s from the precursors without Tween. In contrast, due to the electrostatic interaction between Tween and Cs^+ ions, $Cs_3Cu_2I_5$ is found to form at 42 s, while the $CsCu_2I_3$ appears at 46 s when using precursors with Tween [Fig. 9(e)]. The electrostatic interaction may retard the nucleation rates of both $CsCu_2I_3$ and $Cs_3Cu_2I_5$, facilitating the enhancement of the crystallinity of $CsCu_2I_3/Cs_3Cu_2I_5$ thin films. Thus, the $CsCu_2I_3/Cs_3Cu_2I_5$ thin films with Tween demonstrate excellent morphologies, high surface potential, and favorable energy alignment in emitting devices, enabling the fabrication of WLEDs. Figure 9(f) presents the evolution of the EL spectra, which exhibits the enhanced EL intensity with a negligible change of the emitting wavelength centered at 565 nm when increasing voltages. The WLEDs have a CIE coordinate of (0.44, 0.53) and a

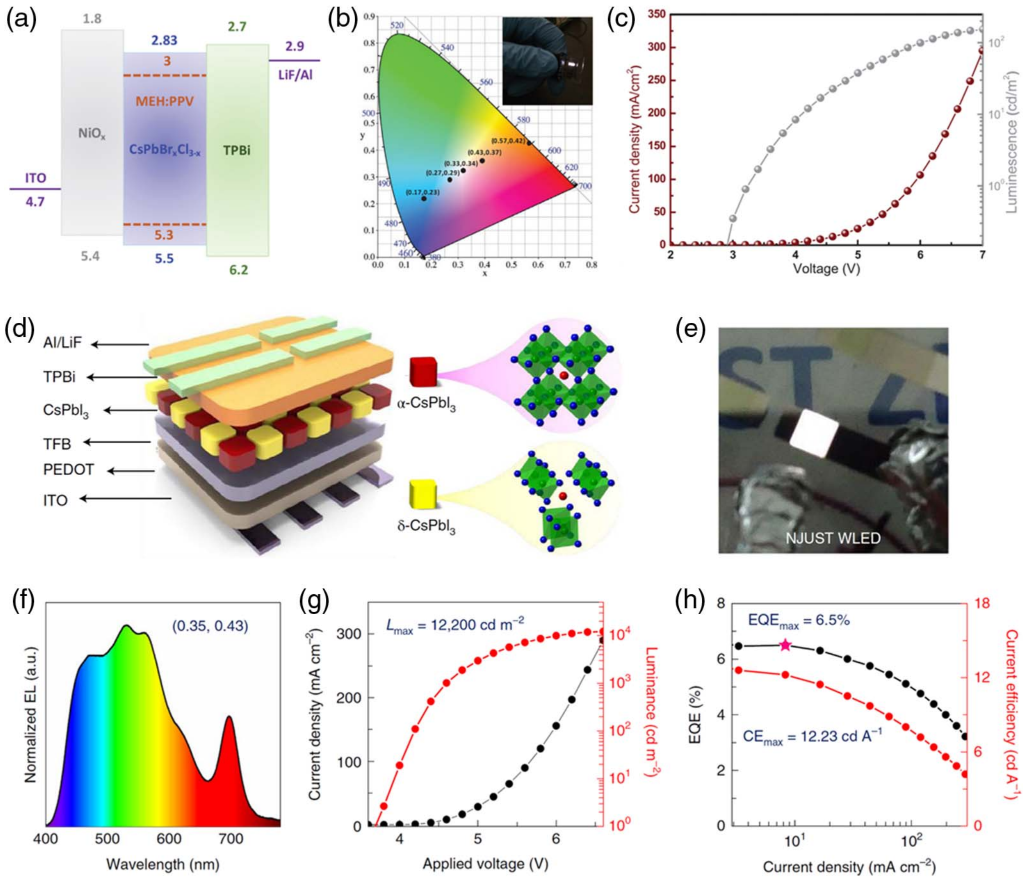

Fig. 8. (a) Energy band schematic, (b) variety of CIE coordinates, and (c) *J-V* and *L-V* curves of electroluminescence WLEDs based on $CsPbBr_xCl_{3-x}$ nanocrystals and MEH:PPV. Reproduced with permission [187]. Copyright 2017, Wiley-VCH GmbH. (d) Schematic of device structure, (e) photograph of an operating device, and (f) EL spectrum of the WLEDs with the emitting of blend of α- and δ–$CsPbI_3$. (g) *J-V* and *L-V* curves, (h) EQE and current efficiency versus current density of the electroluminescence α- and δ–$CsPbI_3$ WLEDs. Reproduced with permission [197]. Copyright 2020, Springer Nature Group.

CCT of 3650 K, corresponding to characters of warm white light. Figures 9(g) and 9(h) plot *J*–*V* and *L*–*V* as well as EQE versus current density curves of WLEDs, showing a maximum luminance and an EQE of 1570 cd/m^2 and 3.1%, respectively. In comparison, WLEDs based on $CsCu_2I_3/Cs_3Cu_2I_5$ thin films without Tween show poor performance with a lower luminance and EQE of 35 cd/m^2 and 0.04%, respectively, indicating the key role of Tween on the optoelectronic performance of WLEDs.

5. VISIBLE LIGHT COMMUNICATION OF IHPS

The continuous development of mobile communication, the Internet of Things (IoT), and supercomputing technologies has led to a rapid growth of data communication, bringing new challenges for efficient and high-speed communication technologies [202]. Owing to the solution processability and low energy consumption, the LEDs-based visible light communication (VLC) is of potential practice in next-generation data communication. With great advances being already achieved in white lighting of IHPs, they are considered suitable candidates as light sources of VLC.

WLEDs based on IHPs were first proposed to serve as light sources in VLC by Bakr *et al.* in 2016 [203]. Figure 10(a) presents the applied VLC system, which includes a source, filters, a lens, and a photodetector. WLEDs consisting of green $CsPbBr_3$ perovskites and red phosphors as excited by blue laser devices are employed as the sources for the VLC system. Although the response frequency of the WLEDs is found to be lower than that of the pure blue laser (1000 MHz), a −3 dB bandwidth of 491.4 MHz is achieved from the WLEDs based on $CsPbBr_3$. This is higher than those based on YAG- and nitride-based phosphors (3–12 MHz) and organic materials (40–200 MHz), implying the outstanding advantages of $CsPbBr_3$ with a fast PL response. As modulated by an on–off keying (OOK) modulation scheme, the bit-error rates (BERs) of the VLC system is 7.4×10^{-5} at 2 Gbit/s, which is lower than the forward error correction (FEC) standard of 3.8×10^{-3}. Furthermore, clear open eyes can be observed in an eye diagram, suggesting the $CsPbBr_3$-based WLEDs enable data transmitting at a high rate of up to 2 Gbit/s, as shown in Fig. 10(b). However, the use of lasers as excited sources may result in the large energy consumption and complicated manufacturing technologies, hindering the development and promotion of IHPs-based WLEDs in VLC.

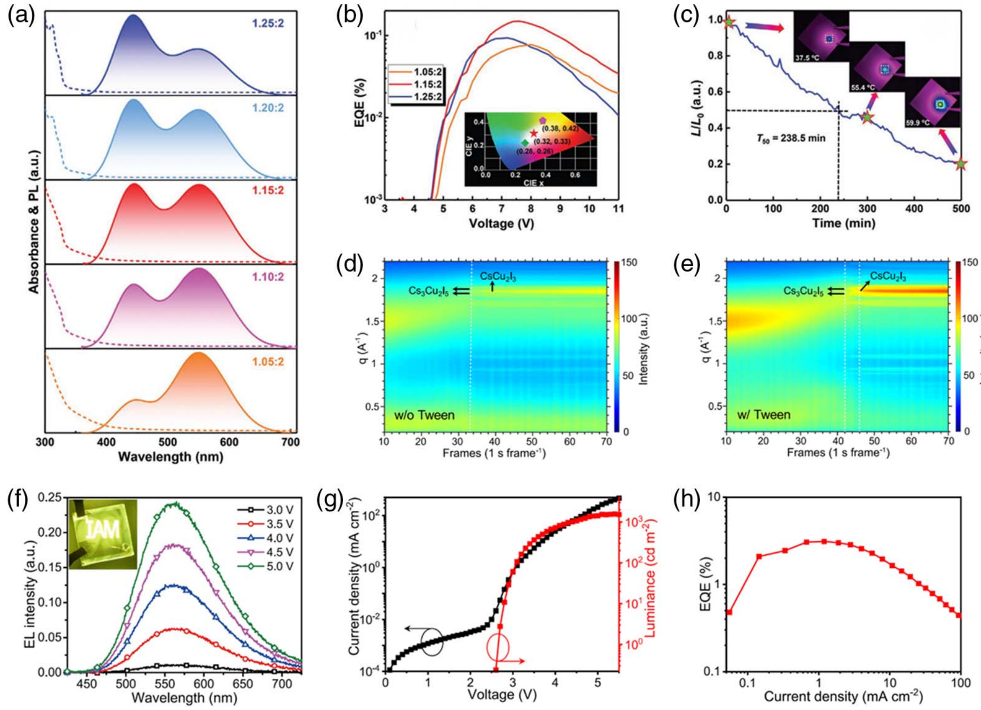

Fig. 9. (a) Absorption and PL spectra of $CsCu_2I_3/Cs_3Cu_2I_5$ thin films with different CsI/CuI ratios. (b) EQE versus voltage curves for the cold, standard, and warm WLEDs. (c) Evolution of the luminance of the WLEDs based on $CsCu_2I_3/Cs_3Cu_2I_5$. Reproduced with permission [198]. Copyright 2021, Wiley-VCH GmbH. Time-resolved GIWAXS profiles of $CsCu_2I_3/Cs_3Cu_2I_5$ thin films (d) without and (e) with Tween. (f) Variety of EL spectra for WLEDs driven at different voltages. (g) *J-V* and *L-V* curves, (h) EQE versus current density curve of WLEDs based on Tween-treated $CsCu_2I_3/Cs_3Cu_2I_5$. Reproduced with permission [200]. Copyright 2021, Springer Nature Group.

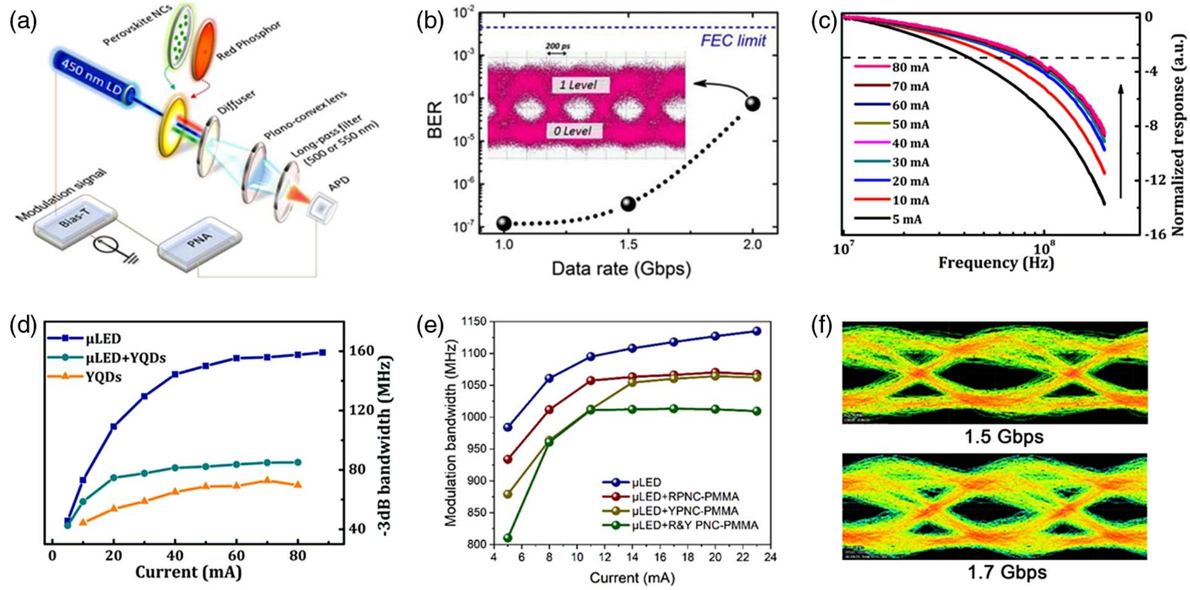

Fig. 10. (a) Schematic of a VLC system. (b) Bit-error rates (BERs) at different data rates, with the forward error correction (FEC) limit labeled. Reproduced with permission [203]. Copyright 2016, American Chemical Society Publications. (c) Response frequencies of WLEDs driven at increased current. (d) Obtained –3 dB bandwidths of μLED chips, WLEDs (μLED chips + yellow quantum dots), and yellow quantum dots as a function of current. Reproduced with permission [204]. Copyright 2018, American Chemical Society Publications. (e) Comparisons of modulation bandwidth (3 dB) of the system based on μLED and μLED with different PNC-PMMA films under various currents. (f) Eye diagram of WLEDs at 1.5 and 1.7 Gbit/s. Reproduced with permission [205]. Copyright 2021, American Chemical Society Publications.

Tian *et al.* prepared WLEDs with yellow $CsPbBr_{1.8}I_{1.2}$ nanocrystals and blue GaN micro-LEDs as lighting sources of VLC [204]. Figure 10(c) presents the frequency response of the modulated WLEDs with the increase of current from 5 to 80 mA. As driven by the rising current, the corresponding −3 dB bandwidth of the VLC increases from ∼40 to ∼80 MHz, which is explained as the reduced carrier lifetime at the higher injection current of devices. However, as shown in Fig. 10(d), a higher −3 dB response is found in pure blue micro-LEDs at the same current, suggesting the further enhancement of the response for VLC is limited by the intrinsic carrier lifetime of $CsPbBr_{1.8}I_{1.2}$ nanocrystals. Besides, the BER results of data communication demonstrate that the BER of the VLC system does not reach the FEC standard at a data rate of 300 Mbit/s. Zhao *et al.* casted a blend of red and green $CsPbX_3$ nanocrystals on blue chips to fabricate WLEDs, which were then applied as light sources in the VLC system [206]. When WLEDs operate at a current density of 7 and 15 kA/cm^2, the modulated −3 dB bandwidth values are 400 and 750 MHz, respectively. These are higher than those of light sources with CdSe/ZnS nanocrystals due to the short PL decay time of $CsPbX_3$ and confirm that IHPs are excellent candidates as emitters in VLC. In 2021, Fu *et al.* fabricated WLEDs with PMMA-coated yellow $CsPb(Br/I)_3$ nanocrystals (YPNCs), red $CsPbI_3$ nanocrystals (RPNCs), and high-bandwidth blue micro-LEDs [205]. As shown in Fig. 10(e), when the driving current is large enough, the bandwidth of the μLED and μLED + R&Y PNC-PMMA reaches 1130 and 1005 MHz, respectively, which are the champions among the previous white-light VLC works based on WLEDs. Moreover, the eye diagrams of the WLEDs operated at a data rate of 1.5 and 1.7 Gbit/s are shown in Fig. 10(f), in which clear open eyes are found, indicating the high-speed operating ability of the VLC system.

Zang *et al.* focused on the improvement of optical efficiency and stability of $CsPbBr_3$ nanocrystals and employed them in the application of VLC [75,77]. The $CsPbBr_3$ nanocrystals were first coated with SiO_x and ZrO_x via a facile solution

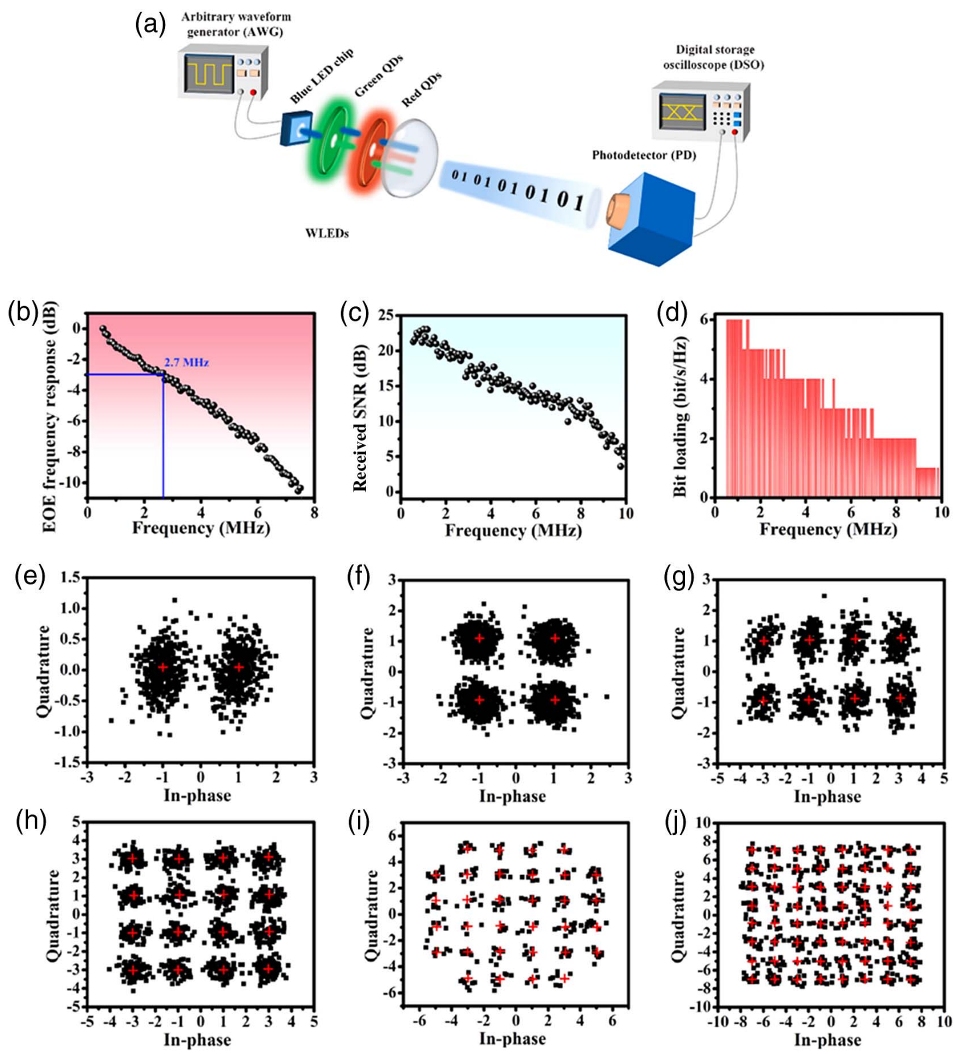

Fig. 11. (a) Schematic diagram of a VLC system. Reproduced with permission [75]. Copyright 2021, Elsevier Publishing Group. (b) Electrical-optical-electrical frequency response, (c) received SNR, (d) bit loading profile of the VLC system based on WLEDs, and the corresponding constellation diagrams of (e) BPSK, (f) 4QAM, (g) 8QAM, (h) 16QAM, (i) 32QAM, and (j) 64QAM, respectively. Reproduced with permission [77]. Copyright 2021, Wiley-VCH GmbH.

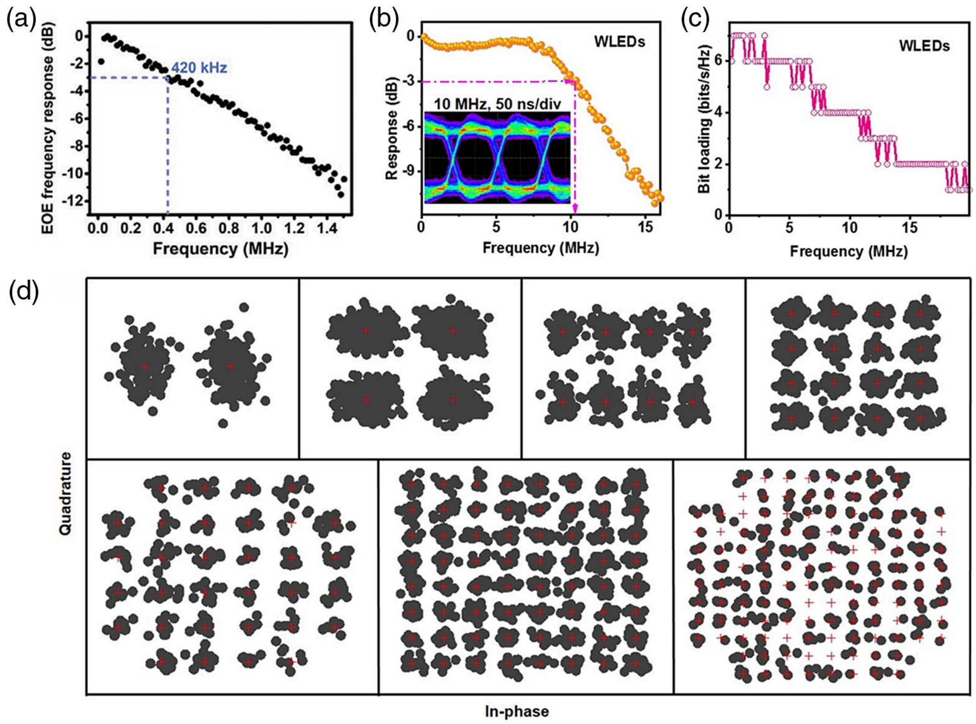

Fig. 12. (a) Electrical-optical-electrical frequency response of WLEDs based on $Cs_3Cu_2Cl_5$ nanocrystals in VLC. Reproduced with permission [207]. Copyright 2021, Wiley-VCH GmbH. (b) Frequency response with the inset showing an eye diagram and (c) bit loading profile of $Cs_3Cu_2I_5/CsCu_2I_3$WLEDs for VLC. (d) Corresponding constellation diagrams of BPSK, 4QAM, 8QAM, 16QAM. 32QAM, 64QAM, and 128QAM [208]. Copyright 2022, Wiley-VCH GmbH.

method and then blended with other emitting materials to contract efficient WLEDs. Figure 11(a) displays a schematic diagram of the VLC system, where the $CsPbBr_3$ nanocrystals and other emitting materials are excited by blue chips to emit white light. The WLEDs based on $CsPbBr_3$ nanocrystals coated with SiO_x and ZrO_x show −3 dB bandwidth of 1.5 and 2.7 MHz [Fig. 11(b)], respectively. Moreover, the signal-to-noise ratio (SNR) of the VLC system is found to reduce gradually as a function of the modulation frequency, as shown in Fig. 11(c). The SNR maintains at least a value of 5 at a modulation frequency of 10 MHz, ensuring the recognizable data communication. Furthermore, the bit loading profile within 10 MHz bandwidth in Fig. 11(d) suggests a highest bit loading of 6 $\text{bit} \cdot \text{s}^{-1} \cdot \text{Hz}^{-1}$ being achieved at lower response frequency and 1 $\text{bit} \cdot \text{s}^{-1} \cdot \text{Hz}^{-1}$ at a modulation frequency as high as 10 MHz. The corresponding received constellation diagrams of binary phase-shift keying (BPSK), 4-ary quadrature amplitude modulation (4QAM), 8QAM, 16QAM, 32QAM, and 64QAM are shown in Figs. 11(e)–11(j), respectively. The transmission data rate of the VLC reaches 33.5 Mbit/s with orthogonal frequency division multiplexing (OFDM) modulation according to the bit loading results, which is ~12 times of the measured −3 dB bandwidth.

Apart from $CsPbX_3$, the WLEDs based on inorganic lead-free perovskites are employable in VLC applications. For example, Zang *et al.* fabricated WLEDs by casting the mix of the silica-coated $Cs_3Cu_2Cl_5$ nanocrystals and phosphors on UV chips and applied them in VLC applications [207]. The −3 dB bandwidth of the VLC is 0.42 MHz, but a high data rate of 2.65 Mbit/s is achieved, as shown in Fig. 12(a). The low bandwidth and communication data rate are ascribed to the long PL decay time of red phosphors in WLEDs and the low luminous efficiency of the white emission. To solve such issues, the same group also employed the prepared high-quality $Cs_3Cu_2I_5$ and $CsCu_2I_3$ single crystals as emitters of white sources in VLC [208]. Owing to the increased PLQY (99.75% for $Cs_3Cu_2I_5$ and 16.73% for $CsCu_2I_3$) and PL decay rates of both single crystals, the corresponding −3 dB bandwidth and achievable communication data rate of the VLC increase to 10.1 MHz and 87.7 Mbit/s, respectively, as shown in Figs. 12(b) and 12(c). Figure 12(d) displays the constellation diagrams of bit loading for the VLC with OFDM modulation, showing the maximum quadrature amplitude modulation of 128 in data communication, which implies the potential applications of WLEDs based on inorganic lead-free perovskites in VLC.

6. CHALLENGES AND FUTURE PERSPECTIVE

As discussed and highlighted in this review, more and more attention has been paid to the research and development of IHPs for lighting and visible light communication. For both inorganic lead halide and lead-free perovskites, various strategies including ligand modification, coating, embedding, and doping have been proposed to improve the optical performance and stability by passivating defects, preventing decomposition, and incorporating novel energy states for emission. Owing to the tunable emission of $CsPbX_3$ perovskites, they are used as emitters to blend with other phosphors and emitting materials to contract efficient photoluminescence and electroluminescence WLEDs. Besides, the inorganic lead-free perovskites with broad emissive spectra, large Stokes shifts, and high PLQYs have been employed in single-component WLEDs without the need of rare-earth phosphors. Furthermore, high-performance WLEDs have been utilized in the VLC applications to act as light sources for outputting light data and showing a high bandwidth response and high communication rates. However, there are research problems and challenges in IHPs as well as their applications in lighting and VLC, which hinder their potential commercialization. Here, the future perspectives to further promote the research and development of lighting and VLC based on IHPs are summarized, focusing on the following challenges.

(1) Owing to the requirement of reducing the use of rare-earth phosphors and achieving high-performance WLEDs with a high CRI, inorganic lead-free perovskites are recognized as good candidates of emitters in single-component WLEDs because of their broad emission with negligible self-absorption derived from the STEs mechanism. However, only very few numbers of lead-free perovskites were reported as emitters for white emission. To realize more possible lead-free perovskites capable of use in WLEDs, a machine-learning method, using the parameters of lead-free perovskites with a variety of structures and components from big data would be developed to filter out those possible choices for the researchers. It would undoubtedly show distinct advantages in the introduction and rapid evolution of lead-free perovskites and attract more attention from researchers to study lead-free perovskites.

(2) The instability of inorganic perovskites in heat, water, polar solvents, and UV irradiation is regarded as the main obstacle hindering their commercialization. To address the problem of instability, the coating and encapsulating strategies are utilized to prevent the inorganic perovskites from water and polar solvents. Generally, stable metal inorganics and polymers can act as the candidates to coat and encapsulate inorganic perovskites, suppressing their decomposition upon heating and UV irradiating treatments.

(3) Despite the advances in photoluminescence WLEDs based on IHPs, they face a series of problems, such as the use of blue/UV chips and rare-earth phosphors, as well as the large energy consumption. It may be attributed to the low-efficiency emissive mechanism of chips-based photoluminescence, in which the current is first injected to drive the emission of chips and then excite the emitters to enable white light. With a direct drive by the current, an increase of the current efficiency and luminance can be achieved in electroluminescence WLEDs. However, the commercialization of electroluminescence WLEDs with organic carrier transporting layers (CTLs) is still limited by the complex manufacturing and high cost. To overcome the problems, the industrialized technologies of organic light-emitting diodes (OLEDs) can be utilized to promote the fabrication of WLEDs based on IHPs. Besides, the progress of low-cost encapsulation technologies can enhance the operating stability of the lighting devices. It is believed that the efficient electroluminescence WLEDs based on IHPs would become mainstreams in lighting fields in this century.

(4) Despite the great advances achieved in electroluminescence WLEDs, their current efficiency and EQE are found to be not relatively high, which is owing to the unbalanced holes/electrons injection and leaky emitting layers. To address the above problems, the thickness of the hole and electron transport layers is optimized and the interlayers are introduced to facilitate balancing the charge injection. Moreover, the additives are incorporated into the precursors of thin films to enable the uniformity of the emitting layers with an efficient crystallinity. Finally, the thermal deposition method and improved coating techniques are also employed to enhance the quality of emitting films.

(5) Although the application and progress of WLEDs based on IHPs in VLC have been achieved in the past years, an achieved bandwidth below 1 GHz still lags far behind that of commercial VLC systems. The low bandwidth of IHPs-based VLC can be attributed to the long luminescent decay time of phosphors and the limited bandwidth of UV and blue chips. To solve such issues, IHPs with rapid luminescence are desired as the emitters in an electroluminescence device structure. Apart from phosphors and blue chips, most of the IHPs exhibit long luminescence decay time, limiting the development of high-speed and high-bandwidth VLC. To enhance the bandwidth and data rates of VLC based on inorganic lead-free perovskites, the emissive inorganic lead-free perovskites with a band-edge and other mechanisms are chosen to act as emitters in sources of VLC. For example, inorganic lead-free $Cs_3Bi_2X_9$ ($X = Cl, Br, I$) with a band-edge and Rb_2AgBr_3 with defect-bound excitons emission exhibit short photoluminescence decay time of 10^0–10^1 ns. These novel lead-free perovskites are regarded as excellent candidates to enhance the performance of VLC. In the meantime, the resistor-capacitance effect in the electroluminescence WLEDs with layered structures needs to be reduced by shrinking the active area and optimizing the energy alignment of devices to decrease both parasitic and charge capacitance originated from the carrier accumulation, respectively.

Funding. National Natural Science Foundation of China (61904023); Fundamental Research Funds for the Central Universities (2021CDJQY-022).

Disclosures. The authors declare that there are no conflicts of interest related to this paper.

Data Availability. Data underlying the results presented in this paper are not publicly available at this time but may be obtained from the authors upon reasonable request.

†These authors contributed equally to this work.

REFERENCES

1. H. Xiang, R. Wang, J. Chen, F. Li, and H. Zeng, "Research progress of full electroluminescent white light-emitting diodes based on a single emissive layer," Light Sci. Appl. **10**, 206 (2021).
2. X. K. Liu, W. Xu, S. Bai, Y. Jin, J. Wang, R. H. Friend, and F. Gao, "Metal halide perovskites for light-emitting diodes," Nat. Mater. **20**, 10–21 (2021).
3. X. Li, X. Gao, X. Zhang, X. Shen, M. Lu, J. Wu, Z. Shi, V. L. Colvin, J. Hu, X. Bai, W. W. Yu, and Y. Zhang, "Lead-free halide perovskites for

light emission: recent advances and perspectives," Adv. Sci. **8**, 2003334 (2021).
4. Z. Chen, Z. Li, T. R. Hopper, A. A. Bakulin, and H. L. Yip, "Materials, photophysics and device engineering of perovskite light-emitting diodes," Rep. Prog. Phys. **84**, 046401 (2021).
5. G. Zhou, B. Su, J. Huang, Q. Zhang, and Z. Xia, "Broad-band emission in metal halide perovskites: mechanism, materials, and applications," Mater. Sci. Eng. R **141**, 100548 (2020).
6. P. Dang, D. Liu, G. Li, A. A. Al Kheraif, and J. Lin, "Recent advances in bismuth ion-doped phosphor materials: structure design, tunable photoluminescence properties, and application in white LEDs," Adv. Opt. Mater. **8**, 1901993 (2020).
7. J. Luo, M. Hu, G. Niu, and J. Tang, "Lead-free halide perovskites and perovskite variants as phosphors toward light-emitting applications," ACS Appl. Mater. Interfaces **11**, 31575–31584 (2019).
8. Y. Wei, Z. Cheng, and J. Lin, "An overview on enhancing the stability of lead halide perovskite quantum dots and their applications in phosphor-converted LEDs," Chem. Soc. Rev. **48**, 310–350 (2019).
9. A. Dey, J. Ye, A. De, E. Debroye, S. K. Ha, E. Bladt, A. S. Kshirsagar, Z. Wang, J. Yin, Y. Wang, L. N. Quan, F. Yan, M. Gao, X. Li, J. Shamsi, T. Debnath, M. Cao, M. A. Scheel, S. Kumar, J. A. Steele, M. Gerhard, L. Chouhan, K. Xu, X. G. Wu, Y. Li, Y. Zhang, A. Dutta, C. Han, I. Vincon, A. L. Rogach, A. Nag, A. Samanta, B. A. Korgel, C. J. Shih, D. R. Gamelin, D. H. Son, H. Zeng, H. Zhong, H. Sun, H. V. Demir, I. G. Scheblykin, I. Mora-Sero, J. K. Stolarczyk, J. Z. Zhang, J. Feldmann, J. Hofkens, J. M. Luther, J. Perez-Prieto, L. Li, L. Manna, M. I. Bodnarchuk, M. V. Kovalenko, M. B. J. Roeffaers, N. Pradhan, O. F. Mohammed, O. M. Bakr, P. Yang, P. Muller-Buschbaum, P. V. Kamat, Q. Bao, Q. Zhang, R. Krahne, R. E. Galian, S. D. Stranks, S. Bals, V. Biju, W. A. Tisdale, Y. Yan, R. L. Z. Hoye, and L. Polavarapu, "State of the art and prospects for halide perovskite nanocrystals," ACS Nano **15**, 10775–10981 (2021).
10. F. Zhou, Z. Li, W. Lan, Q. Wang, L. Ding, and Z. Jin, "Halide perovskite, a potential scintillator for X-ray detection," Small Methods **4**, 2000506 (2020).
11. S. A. Khan, C. Li, A. Jalil, X. Xin, M. Rauf, J. Ahmed, M. A. M. Khan, B. Dong, J. Zhu, and S. Agathopoulos, "Development of structure and tuning ability of the luminescence of lead-free halide perovskite nanocrystals (NCs)," Chem. Eng. J. **420**, 127603 (2021).
12. X. Wang, T. Zhang, Y. Lou, and Y. Zhao, "All-inorganic lead-free perovskites for optoelectronic applications," Mater. Chem. Front. **3**, 365–375 (2019).
13. F. Zhang, J. Song, B. Han, T. Fang, J. Li, and H. Zeng, "High-efficiency pure-color inorganic halide perovskite emitters for ultra-high-definition displays: progress for backlighting displays and electrically driven devices," Small Methods **2**, 1700382 (2018).
14. F. P. Garcia de Arquer, D. V. Talapin, V. I. Klimov, Y. Arakawa, M. Bayer, and E. H. Sargent, "Semiconductor quantum dots: technological progress and future challenges," Science **373**, eaaz8541 (2021).
15. L. Chouhan, S. Ghimire, C. Subrahmanyam, T. Miyasaka, and V. Biju, "Synthesis, optoelectronic properties and applications of halide perovskites," Chem. Soc. Rev. **49**, 2869–2885 (2020).
16. W. Lv, L. Li, M. Xu, J. Hong, X. Tang, L. Xu, Y. Wu, R. Zhu, R. Chen, and W. Huang, "Improving the stability of metal halide perovskite quantum dots by encapsulation," Adv. Mater. **31**, 1900682 (2019).
17. W. Lin, X. Hu, L. Mo, X. Jiang, X. Xing, L. Shui, S. Priya, K. Wang, and G. Zhou, "Progresses on novel B-site perovskite nanocrystals," Adv. Opt. Mater. **9**, 2100261 (2021).
18. H. Huang, L. Polavarapu, J. A. Sichert, A. S. Susha, A. S. Urban, and A. L. Rogach, "Colloidal lead halide perovskite nanocrystals: synthesis, optical properties and applications," NPG Asia Mater. **8**, e328 (2016).
19. F. Igbari, Z. K. Wang, and L. S. Liao, "Progress of lead-free halide double perovskites," Adv. Energy Mater. **9**, 1803150 (2019).
20. M. D. Smith and H. I. Karunadasa, "White-light emission from layered halide perovskites," Acc. Chem. Res. **51**, 619–627 (2018).
21. J. Sun, J. Yang, J. I. Lee, J. H. Cho, and M. S. Kang, "Lead-free perovskite nanocrystals for light-emitting devices," J. Phys. Chem. Lett. **9**, 1573–1583 (2018).
22. H. Yin, Y. Xian, Y. Zhang, W. Li, and J. Fan, "Structurally stabilizing and environment friendly triggers: double-metallic lead-free perovskites," Solar RRL **3**, 1900148 (2019).
23. M. Bidikoudi, E. Fresta, and R. D. Costa, "White perovskite based lighting devices," Chem. Commun. **54**, 8150–8169 (2018).
24. Z. Gao, X. Wang, Y. Bai, C. Sun, H. Liu, L. Wang, S. Su, K. Tian, Z. Zhang, and W. Bi, "High color rendering index and stable white light emitting diodes fabricated from lead bromide perovskites," Appl. Phys. Lett. **115**, 153103 (2019).
25. Y. Deng, X. Lin, W. Fang, D. Di, L. Wang, R. H. Friend, X. Peng, and Y. Jin, "Deciphering exciton-generation processes in quantum-dot electroluminescence," Nat. Commun. **11**, 2309 (2020).
26. Y. Fu, H. Zhu, J. Chen, M. P. Hautzinger, X. Y. Zhu, and S. Jin, "Metal halide perovskite nanostructures for optoelectronic applications and the study of physical properties," Nat. Rev. Mater. **4**, 169–188 (2019).
27. A. Fakharuddin, U. Shabbir, W. Qiu, T. Iqbal, M. Sultan, P. Heremans, and L. Schmidt-Mende, "Inorganic and layered perovskites for optoelectronic devices," Adv. Mater. **31**, 1807095 (2019).
28. N. K. Tailor, S. Kar, P. Mishra, A. These, C. Kupfer, H. Hu, M. Awais, M. Saidaminov, M. I. Dar, C. Brabec, and S. Satapathi, "Advances in lead-free perovskite single crystals: fundamentals and applications," ACS Mater. Lett. **3**, 1025–1080 (2021).
29. S. Zhao, W. Cai, H. Wang, Z. Zang, and J. Chen, "All-inorganic lead-free perovskite(-like) single crystals: synthesis, properties, and applications," Small Methods **5**, 2001308 (2021).
30. Z. Shen, S. Zhao, D. Song, Z. Xu, B. Qiao, P. Song, Q. Bai, J. Cao, G. Zhang, and W. Swelm, "Improving the quality and luminescence performance of all-inorganic perovskite nanomaterials for light-emitting devices by surface engineering," Small **16**, 1907089 (2020).
31. C. H. Lu, G. V. Biesold-McGee, Y. Liu, Z. Kang, and Z. Lin, "Doping and ion substitution in colloidal metal halide perovskite nanocrystals," Chem. Soc. Rev. **49**, 4953–5007 (2020).
32. Y. Liu, Z. Yang, and S. F. Liu, "Recent progress in single-crystalline perovskite research including crystal preparation, property evaluation, and applications," Adv. Sci. **5**, 1700471 (2018).
33. Y. M. Chen, Y. Zhou, Q. Zhao, J. Y. Zhang, J. P. Ma, T. T. Xuan, S. Q. Guo, Z. J. Yong, J. Wang, Y. Kuroiwa, C. Moriyoshi, and H. T. Sun, "$Cs_4PbBr_6/CsPbBr_3$ perovskite composites with near-unity luminescence quantum yield: large-scale synthesis, luminescence and formation mechanism, and white light-emitting diode application," ACS Appl. Mater. Interfaces **10**, 15905–15912 (2018).
34. M. Chen, H. Hu, Y. Tan, N. Yao, Q. Zhong, B. Sun, M. Cao, Q. Zhang, and Y. Yin, "Controlled growth of dodecapod-branched $CsPbBr_3$ nanocrystals and their application in white light emitting diodes," Nano Energy **53**, 559–566 (2018).
35. Y. Wei, K. Li, Z. Cheng, M. Liu, H. Xiao, P. Dang, S. Liang, Z. Wu, H. Lian, and J. Lin, "Epitaxial growth of $CsPbX_3$ (X = Cl, Br, I) perovskite quantum dots via surface chemical conversion of Cs_2GeF_6 double perovskites: a novel strategy for the formation of leadless hybrid perovskite phosphors with enhanced stability," Adv. Mater. **31**, 1807592 (2019).
36. Z. Gong, W. Zheng, Y. Gao, P. Huang, D. Tu, R. Li, J. Wei, W. Zhang, Y. Zhang, and X. Chen, "Full-spectrum persistent luminescence tuning using all-inorganic perovskite quantum dots," Angew. Chem. Int. Ed. **58**, 6943–6947 (2019).
37. T. Xuan, X. Yang, S. Lou, J. Huang, Y. Liu, J. Yu, H. Li, K. L. Wong, C. Wang, and J. Wang, "Highly stable $CsPbBr_3$ quantum dots coated with alkyl phosphate for white light-emitting diodes," Nanoscale **9**, 15286–15290 (2017).
38. M. Su, B. Fan, H. Li, K. Wang, and Z. Luo, "Hydroxyl terminated mesoporous silica-assisted dispersion of ligand-free $CsPbBr_3/Cs_4PbBr_6$ nanocrystals in polymer for stable white LED," Nanoscale **11**, 1335–1342 (2019).
39. D. Yan, S. Zhao, Y. Zhang, H. Wang, and Z. Zang, "Highly efficient emission and high-CRI warm white light-emitting diodes from ligand-modified $CsPbBr_3$ quantum dots," Opto-Electron Adv. **5**, 200075 (2022).
40. P. Wang, X. Bai, C. Sun, X. Zhang, T. Zhang, and Y. Zhang, "Multicolor fluorescent light-emitting diodes based on cesium lead halide perovskite quantum dots," Appl. Phys. Lett. **109**, 063106 (2016).

41. Y. Li, L. Dong, R. Patterson, Z. L. Teh, Y. Hu, S. Huang, and C. Chen, "Stabilizing $CsPbBr_3$ perovskite quantum dots on zirconium phosphate nanosheets through an ion exchange/surface adsorption strategy," Chem. Eng. J. **381**, 122735 (2020).
42. Y. Altintas, I. Torun, A. F. Yazici, E. Beskazak, T. Erdem, M. Serdar Onses, and E. Mutlugun, "Multiplexed patterning of cesium lead halide perovskite nanocrystals by additive jet printing for efficient white light generation," Chem. Eng. J. **380**, 122493 (2020).
43. J. Hao, X. Qu, L. Qiu, G. Li, Y. Wei, G. Xing, H. Wang, C. Yan, H. S. Jang, Z. Cheng, and J. Lin, "One-step loading on natural mineral halloysite nanotube: an effective way to enhance the stability of perovskite $CsPbX_3$ (X = Cl, Br, I) quantum dots," Adv. Opt. Mater. **7**, 1801323 (2018).
44. H. Wu, S. Lin, R. Wang, X. You, and Y. Chi, "Water-stable and ion exchange-free inorganic perovskite quantum dots encapsulated in solid paraffin and their application in light emitting diodes," Nanoscale **11**, 5557–5563 (2019).
45. Q. Pan, H. Hu, Y. Zou, M. Chen, L. Wu, D. Yang, X. Yuan, J. Fan, B. Sun, and Q. Zhang, "Microwave-assisted synthesis of high-quality "all-inorganic" $CsPbX_3$ (X = Cl, Br, I) perovskite nanocrystals and their application in light emitting diodes," J. Mater. Chem. C **5**, 10947–10954 (2017).
46. X. Xu, H. He, Z. Fang, H. Lou, C. Lin, L. Chen, and Z. Ye, "Ultrasonication-assisted ambient-air synthesis of monodispersed blue-emitting $CsPbBr_3$ quantum dots for white light emission," ACS Appl. Nano Mater. **2**, 6874–6879 (2019).
47. M. Chen, Y. Zou, L. Wu, Q. Pan, D. Yang, H. Hu, Y. Tan, Q. Zhong, Y. Xu, H. Liu, B. Sun, and Q. Zhang, "Solvothermal synthesis of high-quality all-inorganic cesium lead halide perovskite nanocrystals: from nanocube to ultrathin nanowire," Adv. Funct. Mater. **27**, 1701121 (2017).
48. T. W. Kang, S. Lee, Y. J. Park, G. J. Jeong, J. S. Kim, B. Bae, J. Hwang, and S. W. Kim, "Enhancement of the optical properties of $CsPbBr_3$ perovskite nanocrystals using three different solvents," Opt. Lett. **45**, 4972–4975 (2020).
49. F. Palazon, F. Di Stasio, Q. A. Akkerman, R. Krahne, M. Prato, and L. Manna, "Polymer-free films of inorganic halide perovskite nanocrystals as UV-to-white color-conversion layers in LEDs," Chem. Mater. **28**, 2902–2906 (2016).
50. G. Li, H. Wang, T. Zhang, L. Mi, Y. Zhang, Z. Zhang, W. Zhang, and Y. Jiang, "Solvent-polarity-engineered controllable synthesis of highly fluorescent cesium lead halide perovskite quantum dots and their use in white light-emitting diodes," Adv. Funct. Mater. **26**, 8478–8486 (2016).
51. X. Li, Y. Wu, S. Zhang, B. Cai, Y. Gu, J. Song, and H. Zeng, "$CsPbX_3$ quantum dots for lighting and displays: room-temperature synthesis, photoluminescence superiorities, underlying origins and white light-emitting diodes," Adv. Funct. Mater. **26**, 2435–2445 (2016).
52. J. Zhou, F. Huang, H. Lin, Z. Lin, J. Xu, and Y. Wang, "Inorganic halide perovskite quantum dot modified YAG-based white LEDs with superior performance," J. Mater. Chem. C **4**, 7601–7606 (2016).
53. H. C. Yoon, H. Kang, S. Lee, J. H. Oh, H. Yang, and Y. R. Do, "Study of perovskite QD down-converted LEDs and six-color white LEDs for future displays with excellent color performance," ACS Appl. Mater. Interfaces **8**, 18189–18200 (2016).
54. F. Fang, W. Chen, Y. Li, H. Liu, M. Mei, R. Zhang, J. Hao, M. Mikita, W. Cao, R. Pan, K. Wang, and X. W. Sun, "Employing polar solvent controlled ionization in precursors for synthesis of high-quality inorganic perovskite nanocrystals at room temperature," Adv. Funct. Mater. **28**, 1706000 (2018).
55. J. Zhang, L. Fan, J. Li, X. Liu, R. Wang, L. Wang, and G. Tu, "Growth mechanism of $CsPbBr_3$ perovskite nanocrystals by a co-precipitation method in a CSTR system," Nano Res. **12**, 121–127 (2018).
56. Y. Cai, L. Wang, T. Zhou, P. Zheng, Y. Li, and R. J. Xie, "Improved stability of $CsPbBr_3$ perovskite quantum dots achieved by suppressing interligand proton transfer and applying a polystyrene coating," Nanoscale **10**, 21441–21450 (2018).
57. Y. Zu, J. Dai, L. Li, F. Yuan, X. Chen, Z. Feng, K. Li, X. Song, F. Yun, Y. Yu, B. Jiao, H. Dong, X. Hou, M. Ju, and Z. Wu, "Ultra-stable $CsPbBr_3$ nanocrystals with near-unity photoluminescence quantum yield via postsynthetic surface engineering," J. Mater. Chem. A **7**, 26116–26122 (2019).
58. G. Almeida, I. Infante, and L. Manna, "Resurfacing halide perovskite nanocrystals," Science **364**, 833–834 (2019).
59. H. Lin, Q. Wei, K. W. Ng, J. Y. Dong, J. L. Li, W. W. Liu, S. S. Yan, S. Chen, G. C. Xing, X. S. Tang, Z. K. Tang, and S. P. Wang, "Stable and efficient blue-emitting $CsPbBr_3$ nanoplatelets with potassium bromide surface passivation," Small **17**, 2101359 (2021).
60. F. Li, Y. Liu, H. Wang, Q. Zhan, Q. Liu, and Z. Xia, "Postsynthetic surface trap removal of $CsPbX_3$ (X = Cl, Br, or I) quantum dots via a ZnX_2/hexane solution toward an enhanced luminescence quantum yield," Chem. Mater. **30**, 8546–8554 (2018).
61. L. Zhang, W. Liang, L. Xu, M. Zhu, X. Wang, J. Su, L. Li, N. Liu, Z. Zhang, and Y. Gao, "Room-temperature quaternary alkylammonium passivation toward morphology-controllable $CsPbBr_3$ nanocrystals with excellent luminescence and stability for white LEDs," Chem. Eng. J. **417**, 129349 (2021).
62. Y. Zhang, G. Li, C. She, S. Liu, F. Yue, C. Jing, Y. Cheng, and J. Chu, "Room temperature preparation of highly stable cesium lead halide perovskite nanocrystals by ligand modification for white light-emitting diodes," Nano Res. **14**, 2770–2775 (2021).
63. S. Chen, Q. Zhong, J. Liu, W. Guan, P. Li, I. Mahmood, M. Cao, and Q. Zhang, "Improved photophysical properties and durability of $CsPbBr_3$ NCs endowed by inorganic oxoacid and bromide ions," Nanoscale **13**, 9634–9640 (2021).
64. C. Gong, X. Wang, X. Xia, X. Yang, L. Wang, and F. Li, "*In-situ* guanidinium bromide passivation treatment of $CsPbBr_3$ perovskite quantum dots exhibiting high photoluminescence and environmental stability," Appl. Surf. Sci. **559**, 149986 (2021).
65. S. Thapa, G. C. Adhikari, H. Zhu, and P. Zhu, "Scalable synthesis of highly luminescent and stable thiocyanate based $CsPbX_3$ perovskite nanocrystals for efficient white light-emitting diodes," J. Alloys Compd. **860**, 158501 (2021).
66. H. Xu, J. Wang, T. Xuan, C. Lv, J. Hou, L. Zhang, Y. Dong, and J. Shi, "Convenient and large-scale synthesis of high-quality, all-inorganic lead halide perovskite nanocrystals for white light-emitting diodes," Chem. Eng. J. **364**, 20–27 (2019).
67. H. Lian, Y. Li, K. Sharafudeen, W. Zhao, G. R. Krishnan, S. Zhang, J. Qiu, K. Huang, and G. Han, "Highly thermotolerant metal halide perovskite solids," Adv. Mater. **32**, 2002495 (2020).
68. T. Liang, W. Liu, X. Liu, Y. Li, W. Wu, and J. Fan, "*In situ* phase-transition crystallization of all-Inorganic water-resistant exciton-radiative heteroepitaxial $CsPbBr_3$-$CsPb_2Br_5$ core-shell perovskite nanocrystals," Chem. Mater. **33**, 4948–4959 (2021).
69. X. Shen, C. Sun, X. Bai, X. Zhang, Y. Wang, Y. Wang, H. Song, and W. W. Yu, "Efficient and stable $CsPb(Br/I)_3$@anthracene composites for white light-emitting devices," ACS Appl. Mater. Interfaces **10**, 16768–16775 (2018).
70. Y. Cai, Y. Li, L. Wang, and R. J. Xie, "A facile synthesis of water-resistant $CsPbBr_3$ perovskite quantum dots loaded poly(methyl methacrylate) composite microspheres based on *in situ* polymerization," Adv. Opt. Mater. **7**, 1901075 (2019).
71. Y. Chang, Y. J. Yoon, G. Li, E. Xu, S. Yu, C. H. Lu, Z. Wang, Y. He, C. H. Lin, B. K. Wagner, V. V. Tsukruk, Z. Kang, N. Thadhani, Y. Jiang, and Z. Lin, "All-inorganic perovskite nanocrystals with a stellar set of stabilities and their use in white light-emitting diodes," ACS Appl. Mater. Interfaces **10**, 37267–37276 (2018).
72. S. Park, M. N. An, G. Almeida, F. Palazon, D. Spirito, R. Krahne, Z. Dang, L. De Trizio, and L. Manna, "$CsPbX_3$/SiO_x (X = Cl, Br, I) monoliths prepared via a novel sol-gel route starting from Cs_4PbX_6 nanocrystals," Nanoscale **11**, 18739–18745 (2019).
73. H. C. Yoon, S. Lee, J. K. Song, H. Yang, and Y. R. Do, "Efficient and stable $CsPbBr_3$ quantum-dot powders passivated and encapsulated with a mixed silicon nitride and silicon oxide inorganic polymer matrix," ACS Appl. Mater. Interfaces **10**, 11756–11767 (2018).
74. Z. Lin, R. Huang, W. Zhang, Y. Zhang, J. Song, H. Li, D. Hou, Y. Guo, C. Song, N. Wan, and P. K. Chu, "Highly luminescent and stable Si-based $CsPbBr_3$ quantum dot thin films prepared by glow discharge plasma with real-time and *in situ* diagnosis," Adv. Funct. Mater. **28**, 1805214 (2018).

75. X. Li, W. Cai, H. Guan, S. Zhao, S. Cao, C. Chen, M. Liu, and Z. Zang, "Highly stable $CsPbBr_3$ quantum dots by silica-coating and ligand modification for white light-emitting diodes and visible light communication," Chem. Eng. J. **419**, 129551 (2021).
76. Y. Jing, M. J. M. Merkx, J. Cai, K. Cao, W. M. M. Kessels, A. J. M. Mackus, and R. Chen, "Nanoscale encapsulation of perovskite nanocrystal luminescent films via plasma-enhanced SiO_2 atomic layer deposition," ACS Appl. Mater. Interfaces **12**, 53519–53527 (2020).
77. Q. Mo, C. Chen, W. Cai, S. Zhao, D. Yan, and Z. Zang, "Room temperature synthesis of stable zirconia-coated $CsPbBr_3$ nanocrystals for white light-emitting diodes and visible light communication," Laser Photon. Rev. **15**, 2100278 (2021).
78. V. Naresh, B. H. Kim, and N. Lee, "Synthesis of $CsPbX_3$ (X = Cl/Br, Br, and Br/I)@SiO_2/PMMA composite films as color-conversion materials for achieving tunable multi-color and white light emission," Nano Res. **14**, 1187–1194 (2020).
79. Y. Jing, K. Cao, B. Zhou, S. Geng, Y. Wen, B. Shan, and R. Chen, "Two-step hybrid passivation strategy for ultrastable photoluminescence perovskite nanocrystals," Chem. Mater. **32**, 10653–10662 (2020).
80. F. Zhang, Z. F. Shi, Z. Z. Ma, Y. Li, S. Li, D. Wu, T. T. Xu, X. J. Li, C. X. Shan, and G. T. Du, "Silica coating enhances the stability of inorganic perovskite nanocrystals for efficient and stable down-conversion in white light-emitting devices," Nanoscale **10**, 20131–20139 (2018).
81. I. Torun, Y. Altintas, A. F. Yazici, E. Mutlugun, and M. S. Onses, "Solid-state encapsulation and color tuning in films of cesium lead halide perovskite nanocrystals for white light generation," ACS Appl. Nano Mater. **2**, 1185–1193 (2019).
82. C. Sun, Y. Zhang, C. Ruan, C. Yin, X. Wang, Y. Wang, and W. W. Yu, "Efficient and stable white LEDs with silica-coated inorganic perovskite quantum dots," Adv. Mater. **28**, 10088–10094 (2016).
83. H. Guan, S. Zhao, H. Wang, D. Yan, M. Wang, and Z. Zang, "Room temperature synthesis of stable single silica-coated $CsPbBr_3$ quantum dots combining tunable red emission of Ag-In-Zn-S for high-CRI white light-emitting diodes," Nano Energy **67**, 104279 (2020).
84. F. Gao, W. Yang, X. Liu, Y. Li, W. Liu, H. Xu, and Y. Liu, "Highly stable and luminescent silica-coated perovskite quantum dots at nanoscale-particle level via nonpolar solvent synthesis," Chem. Eng. J. **407**, 128001 (2021).
85. Y. Lin, X. Zheng, Z. Shangguan, G. Chen, W. Huang, W. Guo, X. Fan, X. Yang, Z. Zhao, T. Wu, and Z. Chen, "All-inorganic encapsulation for remarkably stable cesium lead halide perovskite nanocrystals: toward full-color display applications," J. Mater. Chem. C **9**, 12303–12313 (2021).
86. M. Imran, B. T. Mai, L. Goldoni, M. Cirignano, H. B. Jalali, F. Di Stasio, T. Pellegrino, and L. Manna, "Switchable anion exchange in polymer-encapsulated $APbX_3$ nanocrystals delivers stable all-perovskite white emitters," ACS Energy Lett. **6**, 2844–2853 (2021).
87. J. Y. Sun, F. T. Rabouw, X. F. Yang, X. Y. Huang, X. P. Jing, S. Ye, and Q. Y. Zhang, "Facile two-step synthesis of all-inorganic perovskite $CsPbX_3$ (X = Cl, Br, and I) zeolite-Y composite phosphors for potential backlight display application," Adv. Funct. Mater. **27**, 1704371 (2017).
88. H. Hu, L. Wu, Y. Tan, Q. Zhong, M. Chen, Y. Qiu, D. Yang, B. Sun, Q. Zhang, and Y. Yin, "Interfacial synthesis of highly stable $CsPbX_3$/oxide Janus nanoparticles," J. Am. Chem. Soc. **140**, 406–412 (2018).
89. H. Huang, B. Chen, Z. Wang, T. F. Hung, A. S. Susha, H. Zhong, and A. L. Rogach, "Water resistant $CsPbX_3$ nanocrystals coated with polyhedral oligomeric silsesquioxane and their use as solid state luminophores in all-perovskite white light-emitting devices," Chem. Sci. **7**, 5699–5703 (2016).
90. X. Chen, F. Zhang, Y. Ge, L. Shi, S. Huang, J. Tang, Z. Lv, L. Zhang, B. Zou, and H. Zhong, "Centimeter-sized Cs_4PbBr_6 crystals with embedded $CsPbBr_3$ nanocrystals showing superior photoluminescence: nonstoichiometry induced transformation and light-emitting applications," Adv. Funct. Mater. **28**, 1706567 (2018).
91. S. Ye, J. Y. Sun, Y. H. Han, Y. Y. Zhou, and Q. Y. Zhang, "Confining Mn^{2+}-doped lead halide perovskite in zeolite-Y as ultrastable orange-red phosphor composites for white light-emitting diodes," ACS Appl. Mater. Interfaces **10**, 24656–24664 (2018).
92. W. Yang, F. Gao, Y. Qiu, W. Liu, H. Xu, L. Yang, and Y. Liu, "$CsPbBr_3$-quantum-dots/polystyrene@silica hybrid microsphere structures with significantly improved stability for white LEDs," Adv. Opt. Mater. **7**, 1900546 (2019).
93. Y. Zhao, C. Xie, X. Zhang, and P. Yang, "$CsPbX_3$ quantum dots embedded in zeolitic imidazolate framework-8 microparticles for bright white light-emitting devices," ACS Appl. Nano Mater. **4**, 5478–5485 (2021).
94. B. Li, Y. Zhang, Y. Xu, and Z. Xia, "Design optimization of $CsPbBr_3$ nanocrystals into zeolite beta composites as ultra-stable green emitters for backlight display applications," J. Mater. Chem. C **9**, 12118–12123 (2021).
95. J. Ren, X. Zhou, and Y. Wang, "Dual-emitting $CsPbX_3$@ZJU-28 (X = Cl, Br, I) composites with enhanced stability and unique optical properties for multifunctional applications," Chem. Eng. J. **391**, 123622 (2020).
96. Y. H. Song, S. Y. Park, J. S. Yoo, W. K. Park, H. S. Kim, S. H. Choi, S. B. Kwon, B. K. Kang, J. P. Kim, H. S. Jung, D. H. Yoon, W. S. Yang, and Y. S. Seo, "Efficient and stable green-emitting $CsPbBr_3$ perovskite nanocrystals in a microcapsule for light emitting diodes," Chem. Eng. J. **352**, 957–963 (2018).
97. J. Ren, T. Li, X. Zhou, X. Dong, A. V. Shorokhov, M. B. Semenov, V. D. Krevchik, and Y. Wang, "Encapsulating all-inorganic perovskite quantum dots into mesoporous metal organic frameworks with significantly enhanced stability for optoelectronic applications," Chem. Eng. J. **358**, 30–39 (2019).
98. Y. Wei, H. Xiao, Z. Xie, S. Liang, S. Liang, X. Cai, S. Huang, A. A. Al Kheraif, H. S. Jang, Z. Cheng, and J. Lin, "Highly luminescent lead halide perovskite quantum dots in hierarchical CaF_2 matrices with enhanced stability as phosphors for white light-emitting diodes," Adv. Opt. Mater. **6**, 1701343 (2018).
99. M. N. An, S. Park, R. Brescia, M. Lutfullin, L. Sinatra, O. M. Bakr, L. De Trizio, and L. Manna, "Low-temperature molten salts synthesis: $CsPbBr_3$ nanocrystals with high photoluminescence emission buried in mesoporous SiO_2," ACS Energy Lett. **6**, 900–907 (2021).
100. H. C. Wang, S. Y. Lin, A. C. Tang, B. P. Singh, H. C. Tong, C. Y. Chen, Y. C. Lee, T. L. Tsai, and R. S. Liu, "Mesoporous silica particles integrated with all-inorganic $CsPbBr_3$ perovskite quantum-dot nanocomposites (MP-PQDs) with high stability and wide color Gamut used for backlight display," Angew. Chem. Int. Ed. **55**, 7924–7929 (2016).
101. B. Yang, F. Zheng, S. Mei, Z. Chen, Y. Xie, H. Dai, X. Wei, W. Zhang, F. Xie, J. Ju, Y. Chu, J. Zou, and R. Guo, "Component regulation and crystallization mechanism of $CsPbBr_3$/Cs_4PbBr_6 perovskite composite quantum dots-embedded borosilicate glass for light emitting application," Appl. Surf. Sci. **512**, 145655 (2020).
102. D. Chen, S. Yuan, X. Chen, J. Li, Q. Mao, X. Li, and J. Zhong, "$CsPbX_3$ (X = Br, I) perovskite quantum dot embedded low-melting phosphosilicate glasses: controllable crystallization, thermal stability and tunable emissions," J. Mater. Chem. C **6**, 6832–6839 (2018).
103. Y. Ye, W. Zhang, Z. Zhao, J. Wang, C. Liu, Z. Deng, X. Zhao, and J. Han, "Highly luminescent cesium lead halide perovskite nanocrystals stabilized in glasses for light-emitting applications," Adv. Opt. Mater. **7**, 1801663 (2019).
104. S. Yuan, D. Chen, X. Li, J. Zhong, and X. Xu, "In situ crystallization synthesis of $CsPbBr_3$ perovskite quantum dot-embedded glasses with improved stability for solid-state lighting and random upconverted lasing," ACS Appl. Mater. Interfaces **10**, 18918–18926 (2018).
105. G. Shao, S. Liu, L. Ding, Z. Zhang, W. Xiang, and X. Liang, "$K_xCs_{1-x}PbBr_3$ NCs glasses possessing super optical properties and stability for white light emitting diodes," Chem. Eng. J. **375**, 122031 (2019).
106. D. Chen, Y. Liu, C. Yang, J. Zhong, S. Zhou, J. Chen, and H. Huang, "Promoting photoluminescence quantum yields of glass-stabilized $CsPbX_3$ (X = Cl, Br, I) perovskite quantum dots through fluorine doping," Nanoscale **11**, 17216–17221 (2019).
107. W. Lv, L. Li, M. Li, L. Xu, W. Huang, and R. Chen, "Self-assembly of completely inorganic perovskite nanocrystals with improved stability by anchoring on kaolinite lamellae," Adv. Opt. Mater. **8**, 1901485 (2020).

108. Y. H. Song, S. H. Choi, J. S. Yoo, B. K. Kang, E. K. Ji, H. S. Jung, and D. H. Yoon, "Design of long-term stable red-emitting $CsPb(Br_{0.4}, I_{0.6})_3$ perovskite quantum dot film for generation of warm white light," Chem. Eng. J. **313**, 461–465 (2017).
109. S. Tu, M. Chen, and L. Wu, "Dual-encapsulation for highly stable all-inorganic perovskite quantum dots for long-term storage and reuse in white light-emitting diodes," Chem. Eng. J. **412**, 128688 (2021).
110. Y. T. Hsieh, Y. F. Lin, and W. R. Liu, "Enhancing the water resistance and stability of $CsPbBr_3$ perovskite quantum dots for light-emitting-diode applications through encapsulation in waterproof polymethylsilsesquioxane aerogels," ACS Appl. Mater. Interfaces **12**, 58049–58059 (2020).
111. Y. Wang, Y. Dong, Q. Liu, X. Guo, M. Zhang, and Y. Li, "*In-situ* stabilization strategy for $CsPbX_3$-silicone resin composite with enhanced luminescence and stability," Nano Energy **78**, 105150 (2020).
112. Y. H. Song, J. S. Yoo, B. K. Kang, S. H. Choi, E. K. Ji, H. S. Jung, and D. H. Yoon, "Long-term stable stacked $CsPbBr_3$ quantum dot films for highly efficient white light generation in LEDs," Nanoscale **8**, 19523–19526 (2016).
113. Y. Li, Y. Lv, Z. Guo, L. Dong, J. Zheng, C. Chai, N. Chen, Y. Lu, and C. Chen, "One-step preparation of long-term stable and flexible $CsPbBr_3$ perovskite quantum dots/ethylene vinyl acetate copolymer composite films for white light-emitting diodes," ACS Appl. Mater. Interfaces **10**, 15888–15894 (2018).
114. M. Meyns, M. Peralvarez, A. Heuer-Jungemann, W. Hertog, M. Ibanez, R. Nafria, A. Genc, J. Arbiol, M. V. Kovalenko, J. Carreras, A. Cabot, and A. G. Kanaras, "Polymer-enhanced stability of inorganic perovskite nanocrystals and their application in color conversion LEDs," ACS Appl. Mater. Interfaces **8**, 19579–19586 (2016).
115. H. C. Yoon and Y. R. Do, "Stable and efficient green perovskite nanocrystal-polysilazane films for white LEDs using an electrospray deposition process," ACS Appl. Mater. Interfaces **11**, 22510–22520 (2019).
116. C. Muthu, J. K. Pious, T. Thankachan, N. Krishna, and C. Vijayakumar, "Stable and efficient white photoluminescence from cesium lead halide perovskite nanocrystals/polyfluorene organogel composite by suppressing of halide ion migration," Adv. Opt. Mater. **9**, 2100601 (2021).
117. T. Xuan, J. Huang, H. Liu, S. Lou, L. Cao, W. Gan, R. S. Liu, and J. Wang, "Super-hydrophobic cesium lead halide perovskite quantum dot-polymer composites with high stability and luminescent efficiency for wide color gamut white light-emitting diodes," Chem. Mater. **31**, 1042–1047 (2019).
118. G. C. Adhikari, S. Thapa, H. Zhu, and P. Zhu, "UV resin enhanced stability of metal halide perovskite nanocrystals for white light-emitting diodes," ACS Appl. Electron. Mater. **2**, 35–40 (2019).
119. S. Zhao, Y. Zhang, and Z. Zang, "Room-temperature doping of ytterbium into efficient near-infrared emission $CsPbBr_{1.5}Cl_{1.5}$ perovskite quantum dots," Chem. Commun. **56**, 5811–5814 (2020).
120. B. J. Moon, S. J. Kim, S. Lee, A. Lee, H. Lee, D. S. Lee, T. W. Kim, S. K. Lee, S. Bae, and S. H. Lee, "Rare-earth-element-ytterbium-substituted lead-free inorganic perovskite nanocrystals for optoelectronic applications," Adv. Mater. **31**, 1901716 (2019).
121. J. Shamsi, A. S. Urban, M. Imran, L. De Trizio, and L. Manna, "Metal halide perovskite nanocrystals: synthesis, post-synthesis modifications, and their optical properties," Chem. Rev. **119**, 3296–3348 (2019).
122. Y. Zhao, X. Zhang, C. Xie, W. Shi, P. Yang, and S. P. Jiang, "Controlling Mn emission in $CsPbCl_3$ nanocrystals via ion exchange toward enhanced and tunable white photoluminescence," J. Phys. Chem. C **124**, 27032–27039 (2020).
123. F. Ren, F. Chen, E. Mei, X. Liang, P. Qian, and W. Xiang, "Mg^{2+}-assisted passivation of surface defects of perovskite polymer composite films for white light-emitting diodes," ACS Photon. **8**, 2130–2138 (2021).
124. S. Liu, G. Shao, L. Ding, J. Liu, W. Xiang, and X. Liang, "Sn-doped $CsPbBr_3$ QDs glasses with excellent stability and optical properties for WLED," Chem. Eng. J. **361**, 937–944 (2019).
125. S. Li, Z. Shi, F. Zhang, L. Wang, Z. Ma, D. Yang, Z. Yao, D. Wu, T. T. Xu, Y. Tian, Y. Zhang, C. Shan, and X. J. Li, "Sodium doping-enhanced emission efficiency and stability of $CsPbBr_3$ nanocrystals for white light-emitting devices," Chem. Mater. **31**, 3917–3928 (2019).
126. Q. He, Y. Zhang, Y. Yu, Y. Chen, M. Jin, E. Mei, X. Liang, L. Zhai, and W. Xiang, "Ultrastable Gd^{3+} doped $CsPbBrI_2$ nanocrystals red glass for high efficiency WLEDs," Chem. Eng. J. **411**, 128530 (2021).
127. P. Lin, H. Chen, Z. Wei, Y. Lin, J. Lin, Y. Chen, and Z. Cheng, "Continuous-flow synthesis of doped all-inorganic perovskite nanocrystals enabled by a microfluidic reactor for light-emitting diode application," Sci. China Mater. **63**, 1526–1536 (2020).
128. V. Naresh and N. Lee, "Zn(II)-doped cesium lead halide perovskite nanocrystals with high quantum yield and wide color tunability for color-conversion light-emitting displays," ACS Appl. Nano Mater. **3**, 7621–7632 (2020).
129. H. Ding, W. Liu, Y. Zheng, C. Li, H. Jiang, and X. Wang, "Transition metal halide-doped, highly stable all-inorganic perovskite nanocrystals for fabrication of white light-emitting diodes," J. Mater. Chem. C **7**, 1690–1695 (2019).
130. M. Liu, G. Zhong, Y. Yin, J. Miao, K. Li, C. Wang, X. Xu, C. Shen, and H. Meng, "Aluminum-doped cesium lead bromide perovskite nanocrystals with stable blue photoluminescence used for display backlight," Adv. Sci. **4**, 1700335 (2017).
131. G. C. Adhikari, S. Thapa, H. Zhu, and P. Zhu, "Mg^{2+}-alloyed all-inorganic halide perovskites for white light-emitting diodes by 3D-printing method," Adv. Opt. Mater. **7**, 1900916 (2019).
132. Y. Xie, B. Peng, I. Bravic, Y. Yu, Y. Dong, R. Liang, Q. Ou, B. Monserrat, and S. Zhang, "Highly efficient blue-emitting $CsPbBr_3$ perovskite nanocrystals through neodymium doping," Adv. Sci. **7**, 2001698 (2020).
133. D. Yan, Q. Mo, S. Zhao, W. Cai, and Z. Zang, "Room temperature synthesis of $Sn^{(2+)}$ doped highly luminescent $CsPbBr_3$ quantum dots for high CRI white light-emitting diodes," Nanoscale **13**, 9740–9746 (2021).
134. D. Chen, G. Fang, and X. Chen, "Silica-coated Mn-doped $CsPb(Cl/Br)_3$ inorganic perovskite quantum dots: exciton-to-Mn energy transfer and blue-excitable solid-state Lighting," ACS Appl. Mater. Interfaces **9**, 40477–40487 (2017).
135. X. Tang, W. Chen, Z. Liu, J. Du, Z. Yao, Y. Huang, C. Chen, Z. Yang, T. Shi, W. Hu, Z. Zang, Y. Chen, and Y. Leng, "Ultrathin, core-shell structured SiO_2 coated $Mn^{(2+)}$ -doped perovskite quantum dots for bright white light-emitting diodes," Small **15**, 1900484 (2019).
136. F. Li, Z. Xia, C. Pan, Y. Gong, L. Gu, Q. Liu, and J. Z. Zhang, "High Br^- content $CsPb(Cl_yBr_{1-y})_3$ perovskite nanocrystals with strong Mn^{2+} emission through diverse cation/anion exchange engineering," ACS Appl. Mater. Interfaces **10**, 11739–11746 (2018).
137. W. Chen, T. Shi, J. Du, Z. Zang, Z. Yao, M. Li, K. Sun, W. Hu, Y. Leng, and X. Tang, "Highly stable silica-wrapped Mn-doped $CsPbCl_3$ quantum dots for bright white light-emitting devices," ACS Appl. Mater. Interfaces **10**, 43978–43986 (2018).
138. M. He, Y. Cheng, L. Shen, C. Shen, H. Zhang, W. Xiang, and X. Liang, "Mn-doped $CsPbCl_3$ perovskite quantum dots (PQDs) incorporated into silica/alumina particles used for WLEDs," Appl. Surf. Sci. **448**, 400–406 (2018).
139. H. Wu, S. Xu, H. Shao, L. Li, Y. Cui, and C. Wang, "Single component Mn-doped perovskite-related $CsPb_2Clx_Br_{5-x}$ nanoplatelets with a record white light quantum yield of 49%: a new single layer color conversion material for light-emitting diodes," Nanoscale **9**, 16858–16863 (2017).
140. Y. Yang, Q. Li, Y. Liu, R. Cong, Y. Sun, J. Hou, M. Ge, J. Shi, F. Zhang, G. Zhao, N. Zhang, Y. Fang, and N. Dai, "Magenta-emitting cesium lead halide nanocrystals encapsulated in dimethicone for white light-emitting diodes," ACS Appl. Nano Mater. **3**, 4886–4892 (2020).
141. Y. Zhao, C. Xie, X. Zhang, K. Matras-Postolek, and P. Yang, "Mn: $CsPbBr_3$ nanoplatelets for bright white-emitting displays," ACS Appl. Nano Mater. **4**, 6223–6230 (2021).
142. Y. H. Song, W. B. Kim, J. S. Yoo, S. H. Choi, W. K. Park, Y. Kim, W. S. Yang, D. H. Yoon, and H. S. Jung, "Design of orange-emitting

$CsPb_{0.77}Mn_{0.23}Cl_3$ perovskite film for application in optoelectronic device," Chem. Eng. J. **331**, 803–808 (2018).
143. P. Li, Y. Duan, Y. Lu, A. Xiao, Z. Zeng, S. Xu, and J. Zhang, "Nanocrystalline structure control and tunable luminescence mechanism of Eu-doped $CsPbBr_3$ quantum dot glass for WLEDs," Nanoscale **12**, 6630–6636 (2020).
144. G. Pan, X. Bai, W. Xu, X. Chen, D. Zhou, J. Zhu, H. Shao, Y. Zhai, B. Dong, L. Xu, and H. Song, "Impurity ions codoped cesium lead halide perovskite nanocrystals with bright white light emission toward ultraviolet-white light-emitting diode," ACS Appl. Mater. Interfaces **10**, 39040–39048 (2018).
145. H. Shao, X. Bai, H. Cui, G. Pan, P. Jing, S. Qu, J. Zhu, Y. Zhai, B. Dong, and H. Song, "White light emission in Bi^{3+}/Mn^{2+} ion co-doped $CsPbCl_3$ perovskite nanocrystals," Nanoscale **10**, 1023–1029 (2018).
146. C. Luo, W. Li, J. Fu, and W. Yang, "Constructing gradient energy levels to promote exciton energy transfer for photoluminescence controllability of all-inorganic perovskites and application in single-component WLEDs," Chem. Mater. **31**, 5616–5624 (2019).
147. X. Huang, Q. Sun, and B. Devakumar, "Facile low-temperature solid-state synthesis of efficient blue-emitting $Cs_3Cu_2I_5$ powder phosphors for solid-state lighting," Mater. Today Chem. **17**, 100288 (2020).
148. X. Mo, T. Li, F. Huang, Z. Li, Y. Zhou, T. Lin, Y. Ouyang, X. Tao, and C. Pan, "Highly-efficient all-inorganic lead-free 1D $CsCu_2I_3$ single crystal for white-light emitting diodes and UV photodetection," Nano Energy **81**, 105570 (2021).
149. W. Liu, K. W. Ng, H. Lin, Z. Dai, J. Xu, S. Su, Z. Tang, and S. Wang, "Stable UV-pumped white light-emitting diodes based on anthracene-coated $CsCu_2I_3$," J. Phys. Chem. C **125**, 13076–13083 (2021).
150. T. Jun, K. Sim, S. Iimura, M. Sasase, H. Kamioka, J. Kim, and H. Hosono, "Lead-free highly efficient blue-emitting $Cs_3Cu_2I_5$ with 0D electronic structure," Adv. Mater. **30**, 1804547 (2018).
151. S. Zhao, Q. Mo, W. Cai, H. Wang, and Z. Zang, "Inorganic lead-free cesium copper chlorine nanocrystal for highly efficient and stable warm white light-emitting diodes," Photon. Res. **9**, 187–192 (2021).
152. S. Zhao, S. Jiang, W. Cai, R. Li, Q. Mo, B. Wang, and Z. Zang, "Intrinsic white-light emission from low-dimensional perovskites for white-light-emitting diodes with high-color-rendering index," Cell Rep. Phys. Sci. **2**, 100585 (2021).
153. M. Leng, Y. Yang, K. Zeng, Z. Chen, Z. Tan, S. Li, J. Li, B. Xu, D. Li, M. P. Hautzinger, Y. Fu, T. Zhai, L. Xu, G. Niu, S. Jin, and J. Tang, "All-inorganic bismuth-based perovskite quantum dots with bright blue photoluminescence and excellent stability," Adv. Funct. Mater. **28**, 1704446 (2018).
154. Z. Z. Ma, Z. F. Shi, L. T. Wang, F. Zhang, D. Wu, D. W. Yang, X. Chen, Y. Zhang, C. X. Shan, and X. J. Li, "Water-induced fluorescence enhancement of lead-free cesium bismuth halide quantum dots by 130% for stable white light-emitting devices," Nanoscale **12**, 3637–3645 (2020).
155. Y. Jing, Y. Liu, X. Jiang, M. S. Molokeev, Z. Lin, and Z. Xia, "Sb^{3+} dopant and halogen substitution triggered highly efficient and tunable emission in lead-free metal halide single crystals," Chem. Mater. **32**, 5327–5334 (2020).
156. S. Li, J. Luo, J. Liu, and J. Tang, "Self-trapped excitons in all-inorganic halide perovskites: fundamentals, status, and potential applications," J. Phys. Chem. Lett. **10**, 1999–2007 (2019).
157. P. Vashishtha, G. V. Nutan, B. E. Griffith, Y. Fang, D. Giovanni, M. Jagadeeswararao, T. C. Sum, N. Mathews, S. G. Mhaisalkar, J. V. Hanna, and T. White, "Cesium copper iodide tailored nanoplates and nanorods for blue, yellow, and white emission," Chem. Mater. **31**, 9003–9011 (2019).
158. P. Cheng, L. Sun, L. Feng, S. Yang, Y. Yang, D. Zheng, Y. Zhao, Y. Sang, R. Zhang, D. Wei, W. Deng, and K. Han, "Colloidal synthesis and optical properties of all-inorganic low-dimensional cesium halide nanocrystals," Angew. Chem. Int. Ed. **131**, 16233–16237 (2019).
159. L. Xie, B. Chen, F. Zhang, Z. Zhao, X. Wang, L. Shi, Y. Liu, L. Huang, R. Liu, B. Zou, and Y. Wang, "Highly luminescent and stable lead-free cesium copper halide perovskite powders for UV-pumped phosphor-converted light-emitting diodes," Photon. Res. **8**, 768–775 (2020).
160. R. Lin, Q. Guo, Q. Zhu, Y. Zhu, W. Zheng, and F. Huang, "All-inorganic $CsCu_2I_3$ single crystal with high-PLQY (≈15.7%) intrinsic white-light emission via strongly localized 1D excitonic recombination," Adv. Mater. **31**, 1905079 (2019).
161. R. Fan, S. Fang, C. Liang, Z. Liang, and H. Zhong, "Controllable one-step doping synthesis for the white-light emission of cesium copper iodide perovskites," Photon. Res. **9**, 694–700 (2021).
162. Z. Yang, Z. Jiang, X. Liu, X. Zhou, J. Zhang, and W. Li, "Bright blue light-emitting doped cesium bromide nanocrystals: alternatives of lead-free perovskite nanocrystals for white LEDs," Adv. Opt. Mater. **7**, 1900108 (2019).
163. Z. Li, Z. Rao, Q. Li, L. Zhou, X. Zhao, and X. Gong, "$Cs_2Zr_{1-x}Te_xCl_6$ perovskite microcrystals with ultrahigh photoluminescence quantum efficiency of 79.46% for high light efficiency white light emitting diodes," Adv. Opt. Mater. **9**, 2100804 (2021).
164. Z. Tan, M. Hu, G. Niu, Q. Hu, J. Li, M. Leng, L. Gao, and J. Tang, "Inorganic antimony halide hybrids with broad yellow emissions," Sci. Bull. **64**, 904–909 (2019).
165. G. Xiong, L. Yuan, Y. Jin, H. Wu, Z. Li, B. Qu, G. Ju, L. Chen, S. Yang, and Y. Hu, "Aliovalent doping and surface grafting enable efficient and stable lead-free blue-emitting perovskite derivative," Adv. Opt. Mater. **8**, 2000779 (2020).
166. J. Li, Z. Tan, M. Hu, C. Chen, J. Luo, S. Li, L. Gao, Z. Xiao, G. Niu, and J. Tang, "Antimony doped Cs_2SnCl_6 with bright and stable emission," Front. Optoelectron. **12**, 352–364 (2019).
167. H. Shao, X. Wu, J. Zhu, W. Xu, L. Xu, B. Dong, J. Hu, B. Dong, X. Bai, H. Cui, and H. Song, "Mn^{2+} ions doped lead-free zero-dimensional K_3SbCl_6 perovskite nanocrystals towards white light emitting diodes," Chem. Eng. J. **413**, 127415 (2021).
168. A. Karmakar, G. M. Bernard, A. Meldrum, A. O. Oliynyk, and V. K. Michaelis, "Tailorable indirect to direct band-gap double perovskites with bright white-light emission: decoding chemical structure using solid-state NMR," J. Am. Chem. Soc. **142**, 10780–10793 (2020).
169. Z. Tan, J. Li, C. Zhang, Z. Li, Q. Hu, Z. Xiao, T. Kamiya, H. Hosono, G. Niu, E. Lifshitz, Y. Cheng, and J. Tang, "Highly efficient blue-emitting Bi-doped Cs_2SnCl_6 perovskite variant: photoluminescence induced by impurity doping," Adv. Funct. Mater. **28**, 1801131 (2018).
170. N. R. Wolf, B. A. Connor, A. H. Slavney, and H. I. Karunadasa, "Doubling the stakes: the promise of halide double perovskites," Angew. Chem. Int. Ed. **60**, 16264–16278 (2021).
171. J. H. Wei, J. F. Liao, X. D. Wang, L. Zhou, Y. Jiang, and D. B. Kuang, "All-inorganic lead-free heterometallic $Cs_4MnBi_2Cl_{12}$ perovskite single crystal with highly efficient orange emission," Matter **3**, 892–903 (2020).
172. B. Zhou, Z. Liu, S. Fang, H. Zhong, B. Tian, Y. Wang, H. Li, H. Hu, and Y. Shi, "Efficient white photoluminescence from self-trapped excitons in Sb^{3+}/Bi^{3+}-codoped $Cs_2NaInCl_6$ double perovskites with tunable dual-emission," ACS Energy Lett. **6**, 3343–3351 (2021).
173. D. Manna, T. K. Das, and A. Yella, "Tunable and stable white light emission in Bi^{3+}-alloyed $Cs_2AgInCl_6$ double perovskite nanocrystals," Chem. Mater. **31**, 10063–10070 (2019).
174. J. Luo, X. Wang, S. Li, J. Liu, Y. Guo, G. Niu, L. Yao, Y. Fu, L. Gao, Q. Dong, C. Zhao, M. Leng, F. Ma, W. Liang, L. Wang, S. Jin, J. Han, L. Zhang, J. Etheridge, J. Wang, Y. Yan, E. H. Sargent, and J. Tang, "Efficient and stable emission of warm-white light from lead-free halide double perovskites," Nature **563**, 541–545 (2018).
175. S. Li, Z. Shi, F. Zhang, L. Wang, Z. Ma, D. Wu, D. Yang, X. Chen, Y. Tian, Y. Zhang, C. Shan, and X. Li, "Ultrastable lead-free double perovskite warm-white light-emitting devices with a lifetime above 1000 hours," ACS Appl. Mater. Interfaces **12**, 46330–46339 (2020).
176. M. Hu, J. Luo, S. Li, J. Liu, J. Li, Z. Tan, G. Niu, Z. Wang, and J. Tang, "Broadband emission of double perovskite $Cs_2Na_{0.4}Ag_{0.6}In_{0.995}Bi_{0.005}Cl_6$:$Mn^{2+}$ for single-phosphor white-light-emitting diodes," Opt. Lett. **44**, 4757–4760 (2019).
177. W. Zheng, R. Sun, Y. Liu, X. Wang, N. Liu, Y. Ji, L. Wang, H. Liu, and Y. Zhang, "Excitation management of lead-free perovskite nanocrystals through doping," ACS Appl. Mater. Interfaces **13**, 6404–6410 (2021).
178. C. Y. Wang, P. Liang, R. J. Xie, Y. Yao, P. Liu, Y. Yang, J. Hu, L. Shao, X. W. Sun, F. Kang, and G. Wei, "Highly efficient lead-free

(Bi,Ce)-codoped $Cs_2Ag_{0.4}Na_{0.6}InCl_6$ double perovskites for white light-emitting diodes," Chem. Mater. **32**, 7814–7821 (2020).
179. H. Yin, Q. Kong, R. Zhang, D. Zheng, B. Yang, and K. Han, "Lead-free rare-earth double perovskite $Cs_2AgIn_{1-y-x}Bi_xLa_yCl_6$ nanocrystals with highly efficient warm-white emission," Sci. China Mater. **64**, 2667–2674 (2021).
180. M. Cong, B. Yang, F. Hong, T. Zheng, Y. Sang, J. Guo, S. Yang, and K. Han, "Self-trapped exciton engineering for white-light emission in colloidal lead-free double perovskite nanocrystals," Sci. Bull. **65**, 1078–1084 (2020).
181. Q. Hu, G. Niu, Z. Zheng, S. Li, Y. Zhang, H. Song, T. Zhai, and J. Tang, "Tunable color temperatures and efficient white emission from $Cs_2Ag_{1-x}Na_xIn_{1-y}Bi_yCl_6$ double perovskite nanocrystals," Small **15**, 1903496 (2019).
182. X. Liu, X. Xu, B. Li, L. Yang, Q. Li, H. Jiang, and D. Xu, "Tunable dual-emission in monodispersed Sb^{3+}/Mn^{2+} codoped $Cs_2NaInCl_6$ perovskite nanocrystals through an energy transfer process," Small **16**, 2002547 (2020).
183. J. E. Jeong, J. H. Park, C. H. Jang, M. H. Song, and H. Y. Woo, "Multifunctional charge transporting materials for perovskite light-emitting diodes," Adv. Mater. **32**, 2002176 (2020).
184. W. Zhou, Y. Zhao, X. Zhou, R. Fu, Q. Li, Y. Zhao, K. Liu, D. Yu, and Q. Zhao, "Light-independent ionic transport in inorganic perovskite and ultrastable Cs-based perovskite solar cells," J. Phys. Chem. Lett. **8**, 4122–4128 (2017).
185. J. Xing, Q. Wang, Q. Dong, Y. Yuan, Y. Fang, and J. Huang, "Ultrafast ion migration in hybrid perovskite polycrystalline thin films under light and suppression in single crystals," Phys. Chem. Chem. Phys. **18**, 30484–30490 (2016).
186. H. Cho, Y. H. Kim, C. Wolf, H. D. Lee, and T. W. Lee, "Improving the stability of metal halide perovskite materials and light-emitting diodes," Adv. Mater. **30**, 1704587 (2018).
187. E. P. Yao, Z. Yang, L. Meng, P. Sun, S. Dong, Y. Yang, and Y. Yang, "High-brightness blue and white LEDs based on inorganic perovskite nanocrystals and their composites," Adv. Mater. **29**, 1606859 (2017).
188. C. Y. Huang, S. J. Huang, and M. H. M. Liu, "Hybridization of $CsPbBr_{1.5}I_{1.5}$ perovskite quantum dots with 9,9-dihexylfluorene co-oligomer for white electroluminescence," Org. Electron. **44**, 6–10 (2017).
189. J. Mao, H. Lin, F. Ye, M. Qin, J. M. Burkhartsmeyer, H. Zhang, X. Lu, K. S. Wong, and W. C. H. Choy, "All-perovskite emission architecture for white light-emitting diodes," ACS Nano **12**, 10486–10492 (2018).
190. Y. Wang, L. Yang, H. Chen, C. Liu, W. Liu, H. Xu, C. Zhang, Z. Wang, and Y. Liu, "White LED based on $CsPbBr_3$ nanocrystal phosphors via a facile two-step solution synthesis route," Mater. Res. Bull. **104**, 48–52 (2018).
191. S. Hou, M. K. Gangishetty, Q. Quan, and D. N. Congreve, "Efficient blue and white perovskite light-emitting diodes via manganese doping," Joule **2**, 2421–2433 (2018).
192. C. Wang, D. Xue, X. Shen, H. Wu, Y. Zhang, H. Cui, and W. W. Yu, "White light-emitting devices based on ZnCdS/ZnS and perovskite nanocrystal heterojunction," Nanotechnology **30**, 465201 (2019).
193. S. Chen, C. Chen, C. Bao, M. Mujahid, Y. Li, P. Chen, and Y. Duan, "White light-emitting devices based on inorganic perovskite and organic materials," Molecules **24**, 800 (2019).
194. R. Sun, P. Lu, D. Zhou, W. Xu, N. Ding, H. Shao, Y. Zhang, D. Li, N. Wang, X. Zhuang, B. Dong, X. Bai, and H. Song, "Samarium-doped metal halide perovskite nanocrystals for single-component electroluminescent white light-emitting diodes," ACS Energy Lett. **5**, 2131–2139 (2020).
195. R. R. Rad, A. F. Gualdrón-Reyes, S. Masi, B. A. Ganji, N. Taghavinia, S. Gené-Marimon, E. Palomares, and I. Mora-Seró, "Tunable carbon-$CsPbI_3$ quantum dots for white LEDs," Adv. Opt. Mater. **9**, 2001508 (2020).
196. S. Zhang, L. Yuan, H. Liu, G. Zhou, W. Ding, Z. Qin, X. Li, and S. Wang, "Tunable white light-emitting devices based on unilaminar high-efficiency Zn^{2+}-doped blue $CsPbBr_3$ quantum dots," J. Phys. Chem. Lett. **12**, 8507–8512 (2021).
197. J. Chen, J. Wang, X. Xu, J. Li, J. Song, S. Lan, S. Liu, B. Cai, B. Han, J. T. Precht, D. Ginger, and H. Zeng, "Efficient and bright white light-emitting diodes based on single-layer heterophase halide perovskites," Nat. Photonics **15**, 238–244 (2020).
198. Z. Ma, Z. Shi, D. Yang, Y. Li, F. Zhang, L. Wang, X. Chen, D. Wu, Y. Tian, Y. Zhang, L. Zhang, X. Li, and C. Shan, "High color-rendering index and stable white light-emitting diodes by assembling two broad-band emissive self-trapped excitons," Adv. Mater. **33**, 2001367 (2021).
199. S. Liu, Y. Yue, X. Zhang, C. Wang, G. Yang, and D. Zhu, "A controllable and reversible phase transformation between all-inorganic perovskites for white light emitting diodes," J. Mater. Chem. C **8**, 8374–8379 (2020).
200. H. Chen, L. Zhu, C. Xue, P. Liu, X. Du, K. Wen, H. Zhang, L. Xu, C. Xiang, C. Lin, M. Qin, J. Zhang, T. Jiang, C. Yi, L. Cheng, C. Zhang, P. Yang, M. Niu, W. Xu, J. Lai, Y. Cao, J. Chang, H. Tian, Y. Jin, X. Lu, L. Jiang, N. Wang, W. Huang, and J. Wang, "Efficient and bright warm-white electroluminescence from lead-free metal halides," Nat. Commun. **12**, 1421 (2021).
201. Y. Zhang, Z. Zhang, W. Yu, Y. He, Z. Chen, L. Xiao, J. J. Shi, X. Guo, S. Wang, and B. Qu, "Lead-free double perovskite $Cs_2AgIn_{0.9}Bi_{0.1}Cl_6$ quantum dots for white light-emitting diodes," Adv. Sci. **2**, 2102895 (2021).
202. A. Ren, H. Wang, W. Zhang, J. Wu, Z. Wang, R. V. Penty, and I. H. White, "Emerging light-emitting diodes for next-generation data communications," Nat. Electron. **4**, 559–572 (2021).
203. I. Dursun, C. Shen, M. R. Parida, J. Pan, S. P. Sarmah, D. Priante, N. Alyami, J. Liu, M. I. Saidaminov, M. S. Alias, A. L. Abdelhady, T. K. Ng, O. F. Mohammed, B. S. Ooi, and O. M. Bakr, "Perovskite nanocrystals as a color converter for visible light communication," ACS Photon. **3**, 1150–1156 (2016).
204. S. Mei, X. Liu, W. Zhang, R. Liu, L. Zheng, R. Guo, and P. Tian, "High-bandwidth white-light system combining a micro-LED with perovskite quantum dots for visible light communication," ACS Appl. Mater. Interfaces **10**, 5641–5648 (2018).
205. Z. Wang, Z. Wei, Y. Cai, L. Wang, M. Li, P. Liu, R. Xie, L. Wang, G. Wei, and H. Y. Fu, "Encapsulation-enabled perovskite-PMMA films combining a micro-LED for high-speed white-light communication," ACS Appl. Mater. Interfaces **13**, 54143–54151 (2021).
206. Z. Ma, X. Li, C. Zhang, L. Turyanska, S. Lin, X. Xi, J. Li, T. Hu, J. Wang, A. Patanè, and L. Zhao, "$CsPb(Br/I)_3$ perovskite nanocrystals for hybrid GaN-based high-bandwidth white light-emitting diodes," ACS Appl. Nano Mater. **4**, 8383–8389 (2021).
207. S. Zhao, C. Chen, W. Cai, R. Li, H. Li, S. Jiang, M. Liu, and Z. Zang, "Efficiently luminescent and stable lead-free $Cs_3Cu_2Cl_5$@silica nanocrystals for white light-emitting diodes and communication," Adv. Opt. Mater. **9**, 2100307 (2021).
208. B. Wang, C. Chen, X. Yang, W. Cai, S. Zhao, R. Li, W. Ma, J. Chen, and Z. Zang, "Pressure-assisted cooling to grow ultra-stable $Cs_3Cu_2L_5$ and $CsCu_2L_3$ single crystals for solid-state lighting and visible light communication," EcoMat **4**, e12148 (2022).